Exact actuator disk solutions for non-uniform heavy loading and slipstream contraction

By JOHN T. CONWAY

Agder College, Grimstad, Norway

A semi-analytical method has been developed to solve for the inviscid incompressible flow induced by a heavily loaded actuator disk with non-uniform loading. The solution takes the contraction of the slipstream fully into account. The method is an extension of the analytical theory of Conway (1995) for the linearized actuator disk and is exact for an incompressible perfect fluid. The solutions for the velocities and stream function are given as one-dimensional integrals of expressions containing complete elliptic integrals. Any load distribution with bounded radial gradient can be treated. Results are presented here for both contra-rotating and normal propellers. For the special case of a contra-rotating propeller with a parabolic velocity profile in the ultimate wake, the vorticity in the slipstream is shown to be the same as in the analytically tractable spherical vortex of Hill (1894) and the related family of steady vortices explored by Fraenkel (1970, 1972) and Norbury (1973).

1. Introduction

The actuator disk theory, which originated with the work of Rankine (1865) and Froude (1889), has remained a useful mathematical model for various types of practical propeller calculations in the aeronautical and marine industries, and has also been applied extensively to wind turbines. The original Rankine and Froude theory treated a uniformly loaded actuator disk and much of the subsequent theoretical work on actuator disks has concentrated on the uniformly loaded disk, based on the twin assumptions that it is the simplest case and that it provides a useful paradigm and stepping stone for the generalized disk. It is of course well known that such a uniform load distribution leads to a singular force on the propeller if slipstream rotation is included without introducing a hub. A uniform load distribution on the disk also implies the existence of a vortex sheet at the slipstream boundary which terminates at the rim of the disk. Hough & Ordway (1965) have given the analytical solutions for the velocity fields induced by the linearized disk, and their solution for the radial velocity is singular at the disk rim.

Experience with other related problems involving a terminated vortex sheet (Kaden 1931; Pullin 1978) leads us to expect that such a sheet would roll up into a spiral of infinite complexity in the neighbourhood of the rim, and a local analysis by Schmidt & Sparenberg (1977) for zero free-stream conditions confirms that this is indeed the case, with streamlines passing through the disk more than once near the rim. The importance of this phenomenon for the uniformly loaded disk has also been stressed by van Kuik (1991). While it is very likely that a numerical scheme could be constructed to calculate the essential details of the roll-up, this phenomenon greatly

undermines the simplicity of the uniformly loaded model and the reliability of the elementary formulae derived from it, which are a commonplace of the textbooks. Furthermore, most approaches for the nonlinear generalized actuator disk, such as that of Greenberg & Powers (1970), Greenberg (1972) use the multiple vortex tube approach, where the load distribution is represented as a piecewise-constant distribution with a finite number of vortex sheets being shed from the disk at the radial locations of the discontinuities in the load distribution. These vortex sheets, if treated entirely consistently, would also roll up at their intersections with the disk. Therefore the success of a multiple vortex tube model depends on the non-resolution of this spiral roll-up near the disk, though this is a minor criticism as parallel difficulties exist for all practical methods simulating the roll-up of a free vortex sheet.

In a recent paper, Conway (1995) derived analytical solutions for the entire flow field induced by a linearized actuator disk with essentially arbitrary radial load distribution. The method was based on the construction of the velocities and vector potential of a ring vortex as integrals over the allowed values of the separation constant of the eigensolutions of Laplace's equation in cylindrical coordinates. With this approach a generalized linearized actuator disk with a load distribution which falls continuously to zero at the disk edge can be treated without introducing any free vortex sheets, the slipstream being an axisymmetric volume distribution of vorticity. The velocities calculated by this method were finite and continuous everywhere, even for the case of an elliptic load distribution which has infinite radial slope at the disk rim. The purpose of this article is to present the extension of this method to the generalized nonlinear actuator disk, subject to the important restriction that the vortex density in the slipstream remains bounded. Semi-analytical solutions are presented for the nonlinear actuator disk and an iterative solution procedure applicable to all load distributions with bounded radial gradient. Whereas closed form solutions were obtained for the linearized disk in terms of complete elliptic integrals, the nonlinear solutions are essentially one-dimensional integrals of similar elliptic integral expressions, which are then evaluated numerically, using FORTRAN routines published by Press *et al.* (1992) and Forsythe, Malcolm & Moler (1977).

The restriction to bounded radial gradient of the load distribution, which was not present in the earlier linearized theory (Conway 1995), is a consequence of the numerical content of the present work. It remains to be seen if the theory presented here can be extended in some manner to include load distributions such as the elliptic distribution, which includes a square-root singularity in the radial gradient at the disk rim.

In §2 below the equations governing the nonlinear actuator disk are derived based on a vortex wake model. In §3 it is shown that the case of a contra-rotating propeller with a parabolic radial velocity profile in the ultimate wake is by far the simplest case, for which the azimuthal vorticity in the slipstream is known *a priori* and is in fact the same as that within the spherical vortex of Hill (1894) and the related family of steady vortices explored by Fraenkel (1970, 1972) and Norbury (1973). In §4 a slightly more complex approach for contra-rotating propellers is developed, and in §5 the method is further extended to include single-rotating propellers with swirl. The method allows propeller efficiency to be calculated for specified load distribution and advance ratio and is suitable for coupling to blade element theory to give efficiency as a function of advance ratio for specified propeller geometry. The solution can also be embedded in a suitable panel method to calculate the effect of the propeller's flow field on its vehicle, with slipstream contraction taken fully into account. Table 1 lists the special functions used.

Symbol	Special function
E(k)	Complete elliptic integral of the second kind
$I_{(\lambda,\mu,\nu)}(R, r, z)$	Bessel–Laplace integral
$J_v(x)$	Bessel function of the first kind
K(k)	Complete elliptic integral of the first kind
$\Gamma(x)$	Gamma function
$\delta(x)$	Dirac delta function

TABLE 1. Special functions used

2. General formulation of the problem

A propeller slipstream is a vortical flow region where a scalar potential cannot in general be defined. However for incompressible flow with $\nabla \cdot V = 0$, the velocity field V can be obtained from a vector (solenoidal) potential A through $V = \nabla \times A$. For axisymmetric flows it is convenient to introduce cylindrical polar coordinates (r, ϕ, z), and here the z-axis is specified pointing downstream. Any arbitrary swirl component V_ϕ does not contribute to $\nabla \cdot V$, and therefore a vector potential A can be introduced for the velocity field consisting of the radial and axial components only. In this case A_ϕ is the only non-zero component of A and the axial stream function Ψ is given by rA_ϕ. The vector potential can be constructed such that $\nabla \cdot A = 0$, hence A is given in terms of the vorticity ω of the velocity field $(V_r, 0, V_z)$ by

$$\nabla^2 A = -\omega. \tag{2.1}$$

Only the azimuthal component $\omega_\phi(r, z)$ of ω is non-zero and therefore $A_\phi(r, z)$, $V_r(r, z)$ and $V_z(r, z)$ are fields induced by an axisymmetric ring vortex distribution.

The vector potential and longitudinal velocity fields induced by a ring vortex of strength Γ and radius r' placed with the plane of the ring normal to the z-axis at position z' along the z-axis are (Basset 1888; Lamb 1932; Conway 1995)

$$A_\phi(r, z) = \frac{\Gamma r'}{2} \int_0^\infty J_1(sr')J_1(sr)e^{-s|z-z'|}ds, \tag{2.2}$$

$$V_r(r, z) = \frac{\pm\Gamma r'}{2} \int_0^\infty sJ_1(sr')J_1(sr)e^{-s|z-z'|}ds, \tag{2.3}$$

$$V_z(r, z) = \frac{\Gamma r'}{2} \int_0^\infty sJ_1(sr')J_0(sr)e^{-s|z-z'|}ds. \tag{2.4}$$

In (2.3) above, the positive sign is to be taken for $(z - z') \geqslant 0$ and the minus sign otherwise. These results can be generalized by introducing a ring vortex density function $\gamma(r, z)$, which gives the fields induced by a general axisymmetric ring vortex distribution in the slipstream of an actuator disk placed at $z = 0$ and with slipstream boundary $R(z)$ as

$$A_\phi(r, z) = \frac{1}{2} \int_0^\infty \int_0^{R(z')} \int_0^\infty \gamma(r', z')r'J_1(sr')J_1(sr)e^{-s|z-z'|}ds\,dr'dz', \tag{2.5}$$

$$V_r(r, z) = \frac{1}{2} \int_0^\infty \int_0^{R(z')} \int_0^\infty \pm\gamma(r', z')r'sJ_1(sr')J_1(sr)e^{-s|z-z'|}ds\,dr'dz', \tag{2.6}$$

$$V_z(r,z) = \frac{1}{2}\int_0^\infty \int_0^{R(z')} \int_0^\infty \gamma(r',z')r's J_1(sr')J_0(sr)e^{-s|z-z'|}\mathrm{d}s\,\mathrm{d}r'\mathrm{d}z'. \tag{2.7}$$

Wu (1962) gives the Green's function for the axisymmetric linear operator $\ell \equiv -r\nabla^2$ (operating on the azimuthal component of a vector) as

$$G(r,r',z,z') = \frac{1}{2}\int_0^\infty J_1(sr')J_1(sr)e^{-s|z-z'|}\mathrm{d}s, \tag{2.8}$$

where $G(r,r',z,z')$ is defined such that

$$\ell G(r,r',z,z') = \delta(r-r')\delta(z-z'). \tag{2.9}$$

Hence applying the operator ℓ to both sides of (2.5) gives

$$\nabla^2 A_\phi(r,z) = -\gamma(r,z). \tag{2.10}$$

Comparison of equations (2.1) and (2.10) gives $\gamma(r,z) \equiv \omega_\phi(r,z)$ and the density of the ring vortices is simply the azimuthal component of the vorticity. Therefore a practical scheme for evaluating the vector potential and velocity fields induced by the ring vortex distribution of a propeller slipstream consists of essentially two coupled elements: a means of solving for the vorticity in the propeller slipstream from conditions specified at the actuator disk and a practical means of evaluating the integrals in equations (2.5), (2.6) and (2.7).

2.1. *Determination of the vorticity*

Within a propeller slipstream the steady inviscid incompressible momentum equations can be written in the form

$$\boldsymbol{V} \times \boldsymbol{\omega} = \nabla h, \tag{2.11}$$

where $\boldsymbol{V}$ is the fluid velocity, $\boldsymbol{\omega}$ the vorticity (including the swirl components) and h the specific enthalpy. It follows immediately from (2.11) that $\boldsymbol{V}\cdot\nabla h = 0$ and the axisymmetric stream surfaces are surfaces of constant h, hence $h = h(\Psi)$ where Ψ is the axisymmetric stream function. Therefore (2.11) is equivalent to (Batchelor 1967)

$$\boldsymbol{V} \times \boldsymbol{\omega} = \frac{\mathrm{d}h}{\mathrm{d}\Psi}\nabla\Psi. \tag{2.12}$$

The axial and radial velocity components are given in terms of the stream function by the relations

$$U_\infty + V_z(r,z) = \frac{1}{r}\frac{\partial\Psi(r,z)}{\partial r} \tag{2.13}$$

and

$$V_r(r,z) = -\frac{1}{r}\frac{\partial\Psi(r,z)}{\partial z}, \tag{2.14}$$

where V_z and V_r are the axial and radial perturbation velocities and U_∞ is the undisturbed free-stream velocity. Substituting (2.13) and (2.14) into (2.12) gives the two independent relations below

$$V_r(r,z)\left(\omega_\phi(r,z) + r\frac{\mathrm{d}h}{\mathrm{d}\Psi}\right) = V_\phi(r,z)\omega_r(r,z), \tag{2.15}$$

$$(U_\infty + V_z(r,z))\left(\omega_\phi(r,z) + r\frac{\mathrm{d}h}{\mathrm{d}\Psi}\right) = V_\phi(r,z)\omega_z(r,z). \tag{2.16}$$

These relations can be greatly simplified for the case of an idealized contra-rotating propeller, which is assumed to have no axial gap between the front and rear blade rows and with both sets of blades rotating at the same frequency but in opposite directions. Such a system can impart no mean angular momentum to any flow annulus, therefore V_ϕ is zero everywhere in the slipstream with (2.15) and (2.16) reducing immediately to the relation

$$\frac{\omega_\phi(r,z)}{r} = -\frac{dh}{d\Psi}. \tag{2.17}$$

From Stokes's theorem it follows that ω_z is also zero everywhere and therefore ω_r is zero from vorticity conservation.

For single rotating propellers (2.15) and (2.16) give the relation

$$\omega_r(r,z)(U_\infty + V_z(r,z)) = V_r(r,z)\omega_z(r,z), \tag{2.18}$$

which states that the longitudinal vorticity distribution is aligned with the velocity field consisting of the axial and radial components only. Hence the total longitudinal vorticity enclosed by a stream tube is constant and from Stokes's theorem is related to the total blade circulation Γ by

$$V_\phi(r,z) = -\frac{\Gamma(\Psi)}{2\pi r}, \tag{2.19}$$

where $\Psi(r,0)$ can be determined in the plane of the actuator disk. From vorticity conservation we also have the relation

$$\frac{\omega_z(r,z)}{U_\infty + V_z(r,z)} = g(\Psi). \tag{2.20}$$

Hence substituting (2.18), (2.19) and (2.20) into (2.15) or (2.16) gives the following relations for the vorticity components in the slipstream of a propeller:

$$\omega_\phi(r,z) = -r\frac{dh}{d\Psi} - \frac{\Gamma(\Psi)g(\Psi)}{2\pi r}, \tag{2.21}$$

$$\omega_z(r,z) = (U_\infty + V_z(r,z))g(\Psi), \tag{2.22}$$

$$\omega_r(r,z) = V_r(r,z)g(\Psi). \tag{2.23}$$

In these equations $\Gamma(\Psi)$ is the value of the circulation of the lifting lines of the propeller at $\Psi(r,0)$ and from vorticity conservation the function $g(\Psi)$ can be determined at the actuator disk through the relation

$$\frac{d\Gamma(r,0)}{dr} = -2\pi r\omega_z(r,0), \tag{2.24}$$

so substituting (2.22) into (2.24) gives

$$g(\Psi) = \frac{-d\Gamma(r,0)/dr}{2\pi r(U_\infty + V_z(r,0))}. \tag{2.25}$$

From the chain rule we can write

$$\frac{d\Gamma(r,0)}{dr} = \frac{d\Gamma}{d\Psi}\frac{\partial\Psi(r,0)}{\partial r}, \tag{2.26}$$

hence (2.25) can be simplified to give

$$g(\Psi) = -\frac{1}{2\pi}\frac{d\Gamma}{d\Psi}, \tag{2.27}$$

or alternatively using (2.19) this can be written as

$$g(\Psi) = \frac{d}{d\Psi}(rV_\phi(r,z)).\tag{2.28}$$

All of the elements of (2.21), and hence the vorticity everywhere in the slipstream, can be evaluated from conditions specified in the plane of the actuator disk.

From mass conservation the axial velocity must be continuous across the disk but the other two velocity components are in general discontinuous. If h_0 is the specific enthalpy of the uniform free stream then the specific enthalpy within the slipstream is given by

$$h = h_0 + \frac{\Delta P(r)}{\rho} + \frac{V_\phi^2(r,0+)}{2} + \frac{V_r^2(r,0+) - V_r^2(r,0-)}{2}\tag{2.29}$$

where $\Delta P(r)$ is the pressure jump across the actuator disk and ρ the fluid density. The final term in (2.29) can be written as $\gamma_\phi(r)V_{rm}(r)$ where $\gamma_\phi(r) \equiv (V_r(r,0+) - V_r(r,0-))$ is the azimuthal surface density of vorticity and $V_{rm}(r) \equiv (V_r(r,0+) + V_r(r,0-))/2$ is the mean radial flow component at the disk. The bound surface vorticity of the actuator disk model is the time average of the vorticity contained within the lifting lines of a finite-bladed propeller and therefore $\gamma_\phi(r)$ is zero for propellers with blades which can be represented by straight lifting lines. Many modern propeller blades are indeed either swept back or are S-shaped, and if such blades are represented by lifting lines, these lines will be curved and the blade vorticity will have an azimuthal component. It is to be noted that for contra-rotating propellers with highly swept blades, the contributions to $\gamma_\phi(r)$ from both sets of blades are additive. Applying the Kutta–Joukowski law to the propeller lifting lines and equating the load on the lifting lines with the force produced by $\Delta P(r)$ gives

$$\frac{\Delta P(r)}{\rho} = -\frac{\Gamma(\Psi)}{2\pi}\left(\Omega - V_\phi(r,0+)/2r\right) - \gamma_\phi(r)V_{rm}(r),\tag{2.30}$$

where Ω is the angular velocity of rotation of the propeller blades and $V_\phi(r,0+)/2$ is the induced azimuthal velocity at the propeller lifting lines with the self-influence of the lifting lines excluded. Substituting (2.19) and (2.30) into (2.29) gives (Wu 1962)

$$h(\Psi) = h_0 + \Omega r V_\phi(r,z)\tag{2.31}$$

and hence within the slipstream

$$r\frac{dh}{d\Psi} = \Omega r \frac{d}{d\Psi}(rV_\phi(r,z)).\tag{2.32}$$

From (2.21), (2.28) and (2.32) it follows that the azimuthal component of the vorticity within the slipstream is given by

$$\omega_\phi(r,z) = \left(V_\phi(r,z) - \Omega r\right)\frac{d}{d\Psi}(rV_\phi(r,z)).\tag{2.33}$$

If the bound azimuthal vorticity on the disk surface is included with the volume distribution in the slipstream then the azimuthal vorticity everywhere is given by

$$\omega_\phi(r,z) = \left(V_\phi(r,z) - \Omega r\right)\frac{d}{d\Psi}(rV_\phi(r,z)) + \gamma_\phi(r)\delta(z).\tag{2.34}$$

Substituting (2.34) into (2.1) gives a nonlinear differential equation for Ψ:

$$\frac{\partial^2\Psi}{\partial r^2} - \frac{1}{r}\frac{\partial\Psi}{\partial r} + \frac{\partial^2\Psi}{\partial z^2} = \left(\Omega r^2 - rV_\phi(r,z)\right)\frac{d}{d\Psi}(rV_\phi(r,z)) - r\gamma_\phi(r)\delta(z).\tag{2.35}$$

Equation (2.35) is derived from a rather different point of view in the book by Breslin & Andersen (1994). For propellers with straight lifting lines (2.35) reduces to the equation given by Wu (1962) for the propeller actuator disk:

$$\frac{\partial^2 \Psi}{\partial r^2} - \frac{1}{r}\frac{\partial \Psi}{\partial r} + \frac{\partial^2 \Psi}{\partial z^2} = \left(\Omega r^2 - rV_\phi(r,z)\right)\frac{\mathrm{d}}{\mathrm{d}\Psi}(rV_\phi(r,z)). \tag{2.36}$$

Bragg & Hawthorne (1950) gave a well-known equation for rotary internal flows which in the notation employed here is

$$\frac{\mathrm{d}h}{\mathrm{d}\Psi} = \frac{V_\phi(r,z)}{r}\frac{\mathrm{d}}{\mathrm{d}\Psi}(rV_\phi(r,z)) + \frac{1}{r^2}\left(\frac{\partial^2 \Psi}{\partial r^2} - \frac{1}{r}\frac{\partial \Psi}{\partial r} + \frac{\partial^2 \Psi}{\partial z^2}\right). \tag{2.37}$$

This reduces immediately to (2.36) when combined with (2.31). Bragg & Hawthorne used (2.37) to derive some exact solutions for actuator-disk-driven flow through an annular passage. These solutions are discussed in detail in the book edited by Thwaites (1960) and also in the book by Horlock (1978). However, the internal flow boundary conditions governing these solutions are not applicable to the unrestricted external flow considered here, so these exact solutions are not directly comparable with those presented here, except for special cases in the radial equilibrium limit at downstream infinity where the boundary conditions are essentially equivalent.

When (2.34) is substituted into (2.5), (2.6) and (2.7), we obtain a partial analytical solution of (2.36). In the following sections, only the case of straight lifting lines where $\gamma_\phi(r)$ is zero is treated. The case of swept-back blades can be treated by introducing a finite-strength distribution of bound ring vortices in the plane of the propeller, corresponding to the last term in (2.35). If arbitrary blade shape is allowed, this distribution is also essentially arbitrary. The fields induced by any such 'vortex disk' can be calculated analytically for any realistic variation of $\gamma_\phi(r)$ using the integral of Sonine (1880) and the methods applied by Conway (1995) to the linearized actuator disk.

3. Solution when the vorticity is known

An extremely important special case occurs where the vorticity is known *a priori* everywhere within the slipstream. In equation (2.17) for a contra-rotating propeller it is possible to choose

$$\frac{\mathrm{d}h}{\mathrm{d}\Psi} = -a \tag{3.1}$$

at the propeller disk, where a is a constant. Then equation (2.17) reduces to

$$\omega_\phi = ar \tag{3.2}$$

and the vorticity is known everywhere within the slipstream. The existence of a case where the vorticity is known *a priori* is very important, as the possible existence of vorticity concentration mechanisms suppressed by numerical smearing can be absolutely excluded for this case. The vortex sheet roll-up at the disk rim which leads to the breakdown of the classical uniformly loaded model is just such a mechanism, and (3.2) shows that this phenomenon is not intrinsic to the generalized actuator disk. Equation (3.2) is a special solution of the well-known equation governing the convection of vorticity in an inviscid fluid without swirl (Batchelor 1967)

$$\frac{\mathrm{D}}{\mathrm{Dt}}\left(\frac{\omega_\phi}{r}\right) = 0. \tag{3.3}$$

This distribution of vorticity occurs in the analytically tractable spherical vortex of Hill (1894) and the related family of steady vortex rings explored by Fraenkel (1970, 1972) and Norbury (1973). Equation (3.2) can be immediately solved for the velocity profile in the ultimate wake and gives the parabolic profile

$$V_z(r, \infty) = \frac{a}{2}(R_d^2 - r^2). \tag{3.4}$$

The analytical solutions for the velocity fields and stream function for this case in the lightly loaded limit are given by Conway (1995).

The second exact Bragg & Hawthorne (1950) actuator disk solution assumes that ω_ϕ is a function of r only. For the sub-case of this solution described by (3.2), Horlock (1978) derives a parabolic profile at downstream infinity analogous to (3.4).

Combining (3.2) with (2.5), (2.6) and (2.7) gives after changing the order of integration

$$\Psi(r, z) = \frac{U_\infty r^2}{2} + \frac{ar}{2} \int_0^\infty \int_0^\infty \int_0^{R(z')} r'^2 J_1(sr') J_1(sr) e^{-s|z-z'|} dr' ds\, dz'. \tag{3.5}$$

The radial integration can be performed immediately to give

$$\Psi(r, z) = \frac{U_\infty r^2}{2} + \frac{ar}{2} \int_0^\infty \int_0^\infty R^2(z') \frac{J_2(sR(z')) J_1(sr)}{s} e^{-s|z-z'|} ds\, dz'. \tag{3.6}$$

The integration with respect to s is of the form

$$I_{(\lambda,\mu,\nu)}(R(z'), r, z - z') = \int_0^\infty s^\lambda J_\mu(sR(z')) J_\nu(sr) e^{-s|z-z'|} ds. \tag{3.7}$$

For λ, μ and ν integers, integrals of this form can always be evaluated in terms of complete elliptic integrals using recursion relations derived from standard Bessel function identities (Conway 1995). Hence we have

$$\Psi(r, z) = \frac{U_\infty r^2}{2} + \frac{ar}{2} \int_0^\infty R^2(z') I_{(-1,2,1)}\left(R(z'), r, z - z'\right) dz', \tag{3.8}$$

and similarly the other fields are given by

$$V_z(r, z) = \frac{a}{2} \int_0^\infty R^2(z') I_{(0,2,0)}\left(R(z'), r, z - z'\right) dz' \tag{3.9}$$

and

$$V_r(r, z) = \frac{a}{2} \int_0^\infty \pm R^2(z') I_{(0,2,1)}\left(R(z'), r, z - z'\right) dz'. \tag{3.10}$$

The positive sign in equation (3.10) is to be taken for $z \geqslant z'$ and the negative sign otherwise.

The functions $I_{(-1,2,1)}$, $I_{(0,2,0)}$ and $I_{(0,2,1)}$ are all finite within the slipstream and the integrals (3.8) to (3.10) can be truncated analytically for z' sufficiently large such that $R(z') = R_d$. Hence if the slipstream boundary can be determined, (3.8) to (3.10) can be integrated numerically to give the complete set of fields induced by the actuator disk.

On the slipstream boundary the stream function is constant and equal to the value at the disk rim. Therefore (3.8) gives

$$\Psi(R_a, 0) = \frac{U_\infty R^2(z)}{2} + \frac{aR(z)}{2} \int_0^\infty R^2(z') I_{(-1,2,1)}\left(R(z'), R(z), z - z'\right) \mathrm{d}z'. \qquad (3.11)$$

This equation is a nonlinear, non-singular integral equation for $R(z)$ which can be solved iteratively by successive substitution, as described in the Appendix.

3.1. *Results*

With the introduction of a non-dimensional parameter $\hat{a} \equiv aR_a^2/U_\infty$, then (3.4) becomes

$$\frac{V_z(r, \infty)}{U_\infty} = \frac{\hat{a}}{2R_a^2}\left[R_d^2 - r^2\right]. \qquad (3.12)$$

The propeller wake infinitely far downstream in the annulus between r and $r + \mathrm{d}r$ increases in length by $U_\infty + V_z(r, \infty)$ each second, and the thrust T and the power P for a general propeller without slipstream swirl can be obtained by equating them to the total generation of excess momentum and kinetic energy respectively in the growing slipstream. This gives

$$T = 2\pi\rho \int_0^{Rd} (U_\infty V_z(r, \infty) + V_z^2(r, \infty)) r \, \mathrm{d}r \qquad (3.13)$$

and

$$P = \pi\rho \int_0^{Rd} (2U_\infty^2 V_z(r, \infty) + 3U_\infty V_z^2(r, \infty) + V_z^3(r, \infty)) r \, \mathrm{d}r. \qquad (3.14)$$

Introducing a thrust coefficient C_{Th} based on disk area and a corresponding power coefficient C_P then the propeller efficiency η is given by (Von Mises 1945)

$$\eta \equiv \frac{C_{Th}}{C_P}, \quad \text{where} \quad C_{Th} \equiv \frac{2T}{\pi\rho U_\infty^2 R_a^2} \quad \text{and} \quad C_P \equiv \frac{2P}{\pi\rho U_\infty^3 R_a^2}.$$

With these definitions, substituting (3.12) into (3.13) and (3.14) gives

$$C_{Th} = \frac{\hat{a}}{2}\left(\frac{R_d}{R_a}\right)^4 \left[1 + \frac{\hat{a}}{3}\left(\frac{R_d}{R_a}\right)^2\right] \qquad (3.15)$$

and

$$C_P = \frac{\hat{a}}{2}\left(\frac{R_d}{R_a}\right)^4 \left[1 + \frac{\hat{a}}{2}\left(\frac{R_d}{R_a}\right)^2 + \frac{\hat{a}^2}{16}\left(\frac{R_d}{R_a}\right)^4\right], \qquad (3.16)$$

hence

$$\eta = \frac{1 + \hat{a}(R_d/R_a)^2/3}{1 + \hat{a}(R_d/R_a)^2/2 + \hat{a}^2(R_d/R_a)^4/16}. \qquad (3.17)$$

Defining $\bar{v}$ as the mean downstream perturbation velocity in the slipstream (normalized by U_∞) then (3.17) can be written concisely as

$$\eta = \frac{1 + 4\bar{v}/3}{(1 + \bar{v})^2}. \qquad (3.18)$$

The corresponding formula for the ideal efficiency η_i of the uniformly loaded disk can be derived in the same fashion by considering the momentum and energy generation
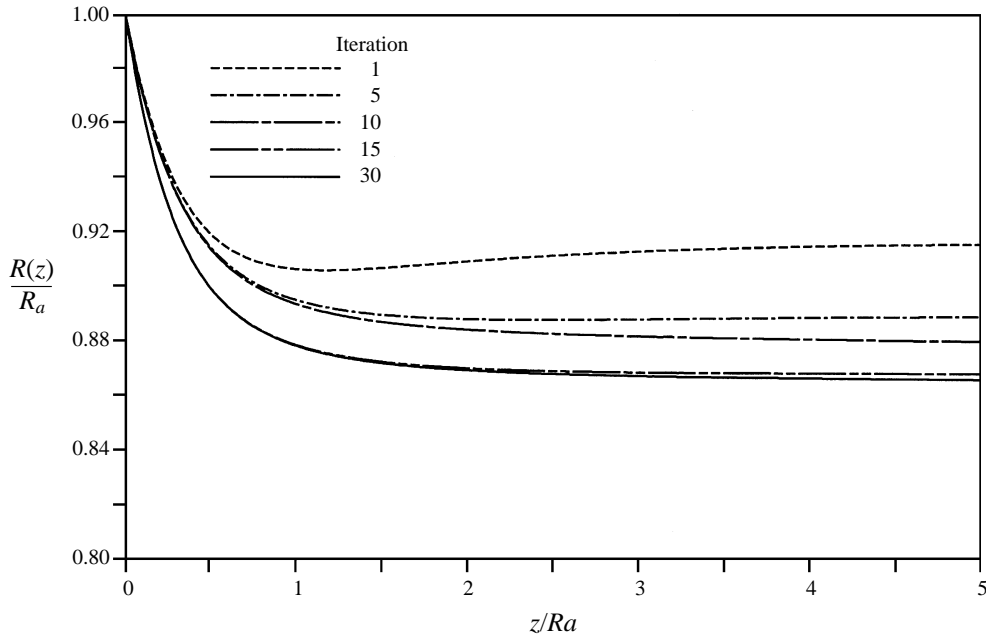
FIGURE 1. Convergence of the slipstream boundary for $\hat{a} = 4$ ($C_{Th} = 2.445$).

in the downstream limit, which gives

$$\eta_i = \frac{2}{2 + \bar{v}}. \qquad (3.19)$$

Although this result is familiar from elementary theory, its derivation from (3.13) and (3.14) establishes (3.19) as an exact relation independent of Froude's propeller law and despite the shortcomings of the elementary theory discussed in §1.

In order to determine the thrust, power and efficiency from (3.20) to (3.22) for given $\hat{a}$ or for specified C_{Th}, equation (3.11) must be solved to obtain the slipstream contraction (R_d/R_a) for the given value of $\hat{a}$. The convergence of the iteration to solve (3.11) is extremely rapid for moderate values of $\hat{a}$ but degrades with increasing $\hat{a}$ and for large values of $\hat{a}$ much above 5, under-relaxation is needed to stabilize the iteration. Figure 1 shows the convergence of the slipstream boundary without under-relaxation for $\hat{a} = 4$, which corresponds to a realistic thrust coefficient $C_{Th} = 2.445$ and a slipstream contraction (R_d/R_a) = 0.8804. For this value of $\hat{a}$ a solution can be obtained with much fewer iterations using under-relaxation. The slipstream has essentially reached its final converged limit within two propeller diameters downstream of the disk. The converged slipstream contraction shown in figure 1 is qualitatively similar to those obtained with the nonlinear actuator disk model of Greenberg & Powers (1970).

Figure 2 shows the converged slipstream boundaries for $a = -1, 2, 5, 10$ and 20, which correspond to thrust coefficients $C_{Th} = -0.4484, 1.131, 3.147, 6.940$ and 15.02, and slipstream contractions (R_d/R_a) = 1.111, 0.9218, 0.8651 and 0.7499 respectively. For values of $\hat{a}$ of 5 and above, under-relaxation was used to obtain the solutions. The distance downstream where some specified fraction of the final slipstream contraction is achieved decreases markedly as C_{Th} is increased.

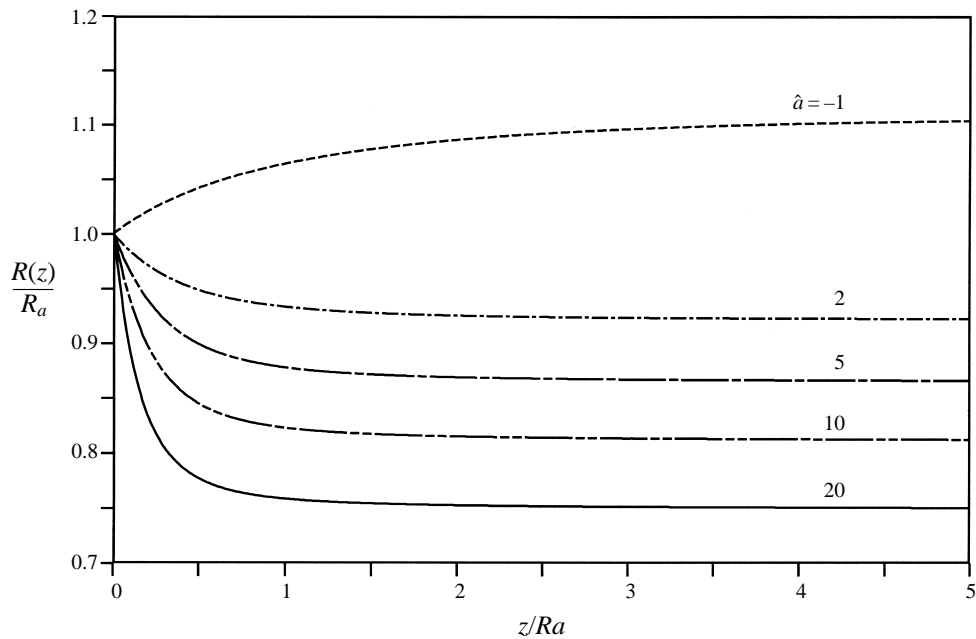Figures 3(a) and 3(b) show the final slipstream contraction and the efficiency η

FIGURE 2. Converged slipstream boundaries for $\hat{a} = -1, 2, 5, 10$ and 20. This corresponds to $C_{Th} = -0.4484, 1.131, 3.147, 6.940$ and 15.02 repectively.

respectively as functions of C_{Th} for this actuator disk compared with the elementary textbook formulae (Von Mises 1945)

$$\frac{R_d}{R_a} = \left[\frac{1 + (1 + C_{Th})^{1/2}}{2(1 + C_{Th})^{1/2}} \right]^{1/2} \tag{3.20}$$

and

$$\eta_i = \frac{2}{1 + (1 + C_{Th})^{1/2}}. \tag{3.21}$$

These elementary formulae are based on Froude's (1889) propeller law, which states that a uniform perturbation velocity is induced at the disk which is exactly half the final perturbation velocity induced in the slipstream at downstream infinity. The efficiency η is of course somewhat less than the ideal efficiency, and the contraction of the slipstream reaches a greater final value for larger values of C_{Th}. The slipstream contraction is rather better predicted by (3.20) for moderate values of C_{Th} than the efficiency.

Figure 4 compares the induced axial velocity $V_z(r, z)$ for $\hat{a} = 5$ ($C_{Th} = 3.147$) at various values of the axial coordinate z. The distributions are qualitatively similar to the corresponding results for the linearized disk (Conway 1995), apart from the explicit slipstream contraction and the fact that the induced axial velocity close to the edge of the disk is negative, though the total axial component at the disk is always positive.
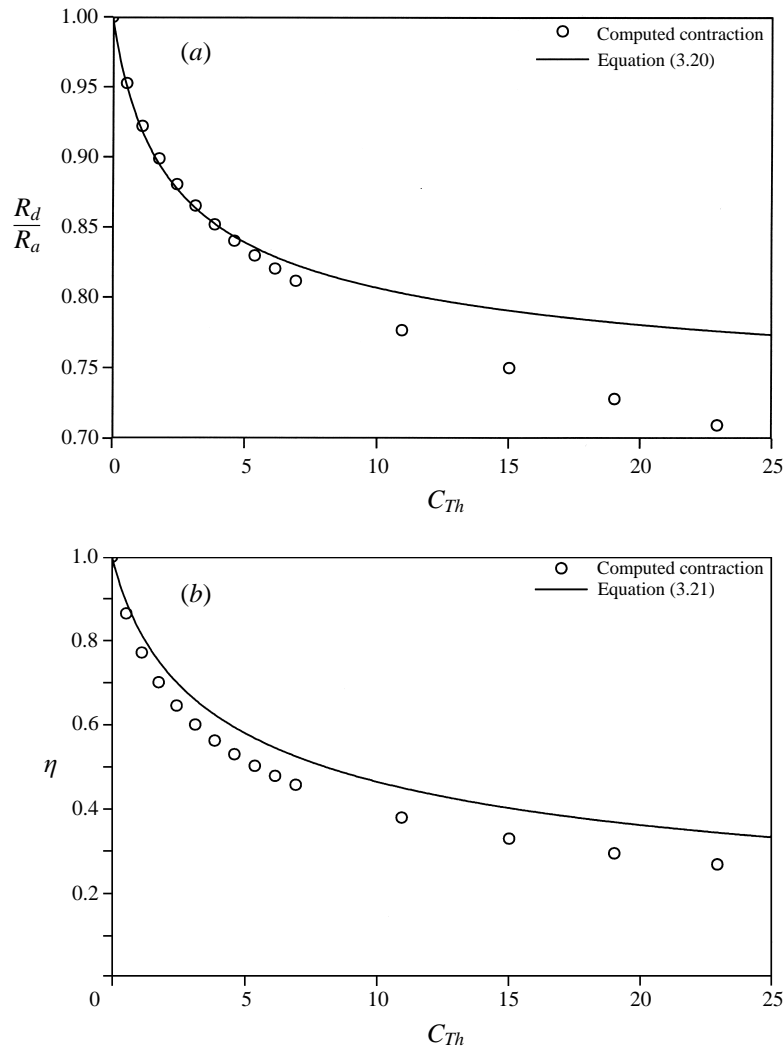
FIGURE 3. (*a*) Slipstream contraction R_d/R_a vs. C_{Th}. (*b*) Efficiency η vs. C_{Th}.

The non-dimensional axial velocity ratio $V_z(0,z)/V_z(0,\infty)$ in the lightly loaded limit (Conway 1995) is

$$\frac{V_z(0,z)}{V_z(0,\infty)} = \frac{1}{2} + \frac{z}{R_a}\left[\left(1+\left(\frac{z}{R_a}\right)^2\right)^{1/2} - \frac{|z|}{R_a}\right]. \qquad (3.22)$$

Figure 5 compares (3.22) with the nonlinear results for various values of C_{Th}. There is some deviation from (3.22) both in front of the disk and behind it, though perhaps less than might be expected for very large values of C_{Th}. Figure 6 shows the variation of $V_z(0,0)/V_z(0,\infty)$ with C_{Th} and illustrates the extent to which Froude's propeller law holds in the nonlinear case. Clearly this law, though rigorously true for the linearized disk, is rather approximate for realistic values of C_{Th}, for which the axial velocity at the disk reaches perhaps 55% of its downstream value. The increase of
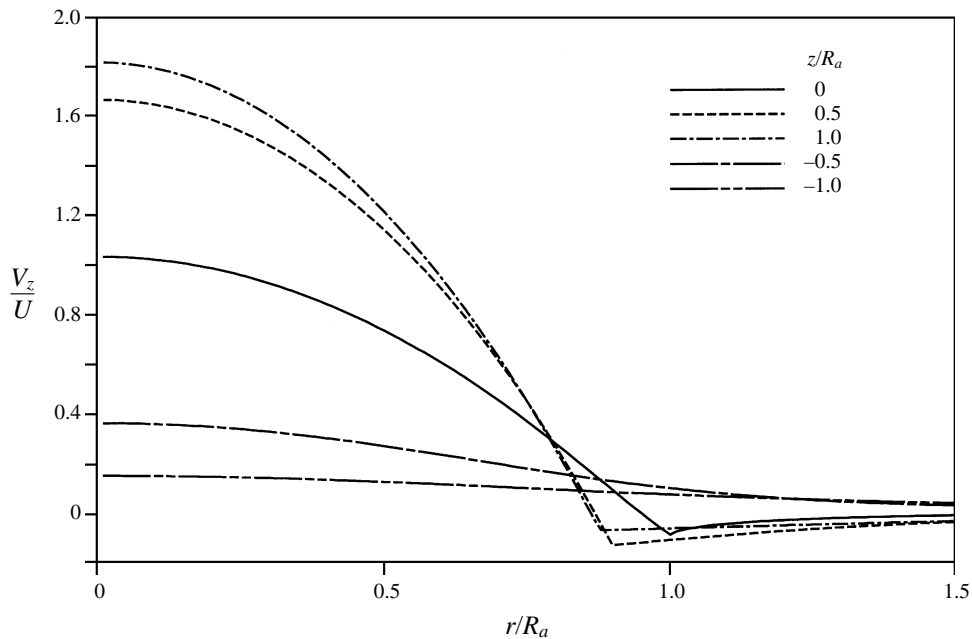
FIGURE 4. Induced axial velocity $V_z(r,z)$ as a function of the radial coordinate r at various values of the axial coordinate z for $\hat{a} = 5$ ($C_{Th} = 3.147$).

$V_z(0,0)/V_z(0,\infty)$ with C_{Th} is consistent with more rapid slipstream contraction as C_{Th} is increased.

Figure 7 shows the radial velocity in the actuator disk plane and at several axial locations fore and aft of this plane for $\hat{a} = 5$ ($C_{Th} = 3.147$). For the linearized disk there is fore-and-aft symmetry of V_r about the actuator disk plane (Conway 1995), and this symmetry is broken for the nonlinear disk. As was found by Conway (1995) for the linearized disk, the radial velocity in the actuator disk plane is of the same order as the induced axial component, and in this case both are comparable in magnitude with the free stream. Another difference between the linearized and nonlinear cases is the discontinuity in the slope of V_r at the slipstream boundary. For the linearized actuator disk (Conway 1995) there is such a discontinuity in the slope of the axial perturbation velocity V_z at the cylindrical boundary between vortical and potential flow, but not for the radial component V_r. The difference results because the boundary between the vortical and non-vortical flow regions (the slipstream boundary) is no longer parallel to the z-axis for the nonlinear case. From (2.14) it follows that V_r is determined by the gradient of Ψ parallel to the z-axis. On traversing a path parallel to the z-axis which cuts the slipstream boundary, a finite discontinuity in ω_ϕ is encountered at the boundary. This necessarily results in a corresponding finite discontinuity in $\partial V_r/\partial r$.

The radial load distribution can be obtained from (2.29) and integration of (3.1) using the boundary condition of zero load at the disk rim. If a non-dimensional load distribution $L(r)$ is defined by

$$L(r) = \frac{2\Delta P(r)}{\rho U_\infty^2} \tag{3.23}$$

then

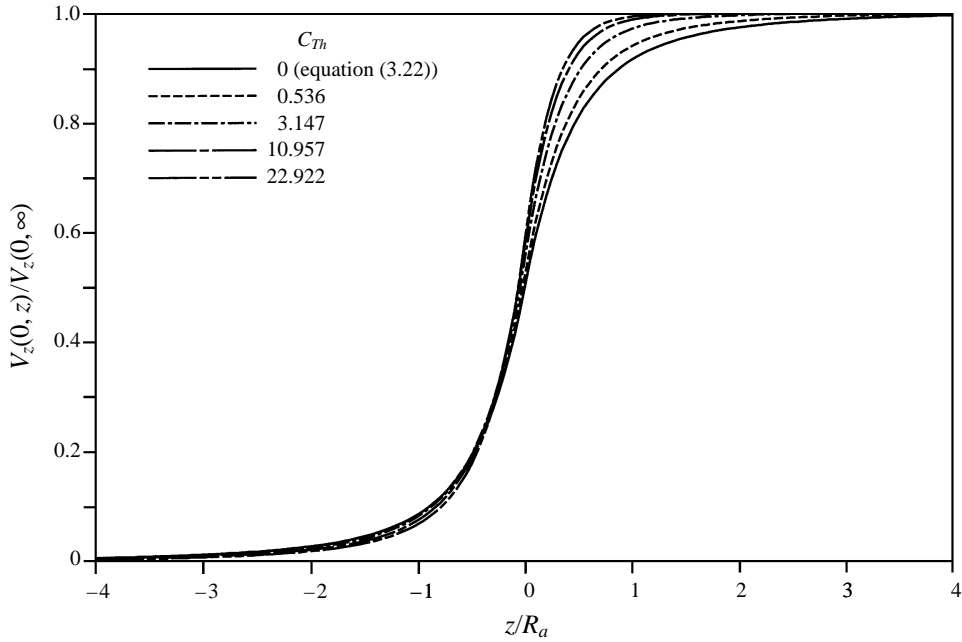$$L(r) = \frac{2\hat{a}(\Psi_e - \Psi(r,0))}{U_\infty R_a^2} \tag{3.24}$$

FIGURE 5. Axial velocity ratio $V_z(0,z)/V_z(0,\infty)$ vs. z for various values of C_{Th} compared with the linearized result from equation (3.22).
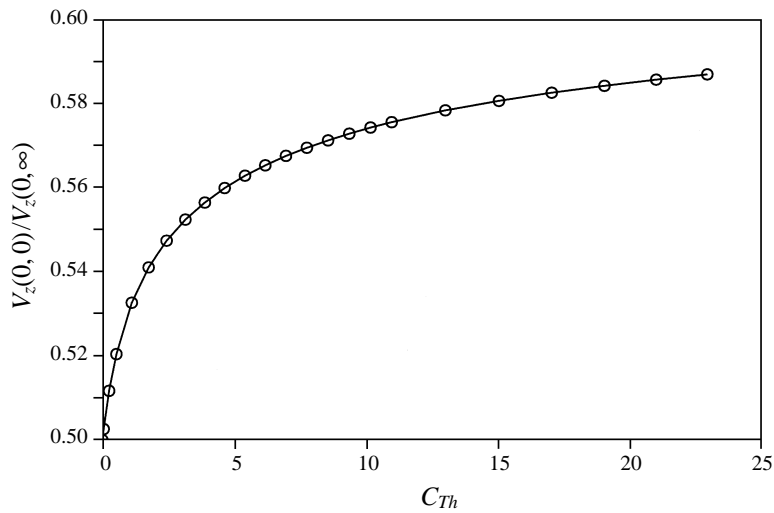

FIGURE 6. Axial velocity ratio $V_z(0,0)/V_z(0,\infty)$ as a function of C_{Th}.

where Ψ_e is the value of the stream function at the edge of the disk, and a normalized distribution is given by

$$\frac{L(r)}{L(0)} = 1 - \frac{\Psi(r,0)}{\Psi_e}. \tag{3.25}$$

Normalized load distributions for various values of C_{Th} are shown in figure 8. For large values of C_{Th} there is some distortion from the purely parabolic load distribution of the linearized case.
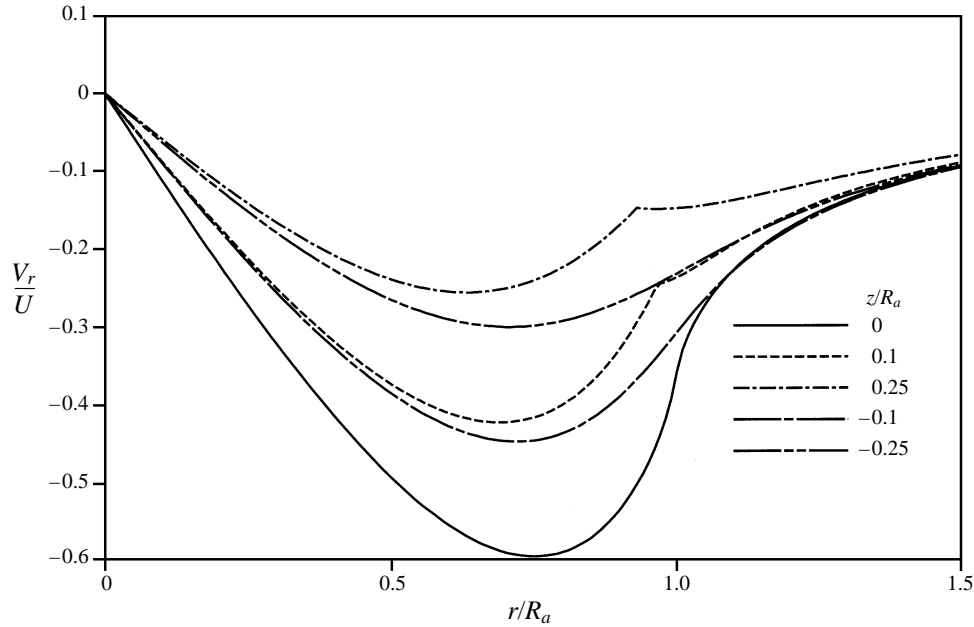
FIGURE 7. Radial velocity $V_r(r,z)$ as a function of the radial coordinate r at various axial stations fore and aft of the disk for $\hat{a} = 5$ ($C_{Th} = 3.147$).

4. Generalized propellers without slipstream rotation

For a contra-rotating propeller or a single-rotating propeller in the approximation where swirl is neglected, (2.29) can be written as

$$h(\Psi) = h_0 + \frac{\Delta P}{\rho}. \tag{4.1}$$

Provided the load distribution has finite slope everywhere, we can represent $h(\Psi)$ everywhere within the slipstream to any required accuracy by a polynomial in Ψ/Ψ_e:

$$h(\Psi) = h_0 + \sum_{m=0}^{M} a_m \left(\frac{\Psi}{\Psi_e} \right)^m. \tag{4.2}$$

At the slipstream edge $h(\Psi) = h_0$ so $\sum_{m=0}^{M} a_m = 0$, and if the load distribution also falls to zero at the blade roots we also have $a_0 = 0$ and therefore $\sum_{m=1}^{M} a_m = 0$. From (2.17) and (4.2) we have

$$\frac{\omega_\phi}{r} = -\sum_{m=1}^{M} \frac{m a_m}{\Psi_e} \left(\frac{\Psi}{\Psi_e} \right)^{m-1}, \tag{4.3}$$

and in the downstream limit, $\omega_\phi = -\mathrm{d}V_z(r,\infty)/\mathrm{d}r$ so from (2.13) and (4.3) we obtain the ordinary differential equation for the ultimate wake

$$\frac{1}{r} \frac{\mathrm{d}}{\mathrm{d}r} \left(\frac{1}{r} \frac{\mathrm{d}\Psi}{\mathrm{d}r} \right) = \sum_{m=1}^{M} \frac{m a_m}{\Psi_e} \left(\frac{\Psi}{\Psi_e} \right)^{m-1}. \tag{4.4}$$

Once the final contracted slipstream radius R_d or the mass flow through the disk have been determined, this equation can always be integrated by a suitable Runge–Kutta
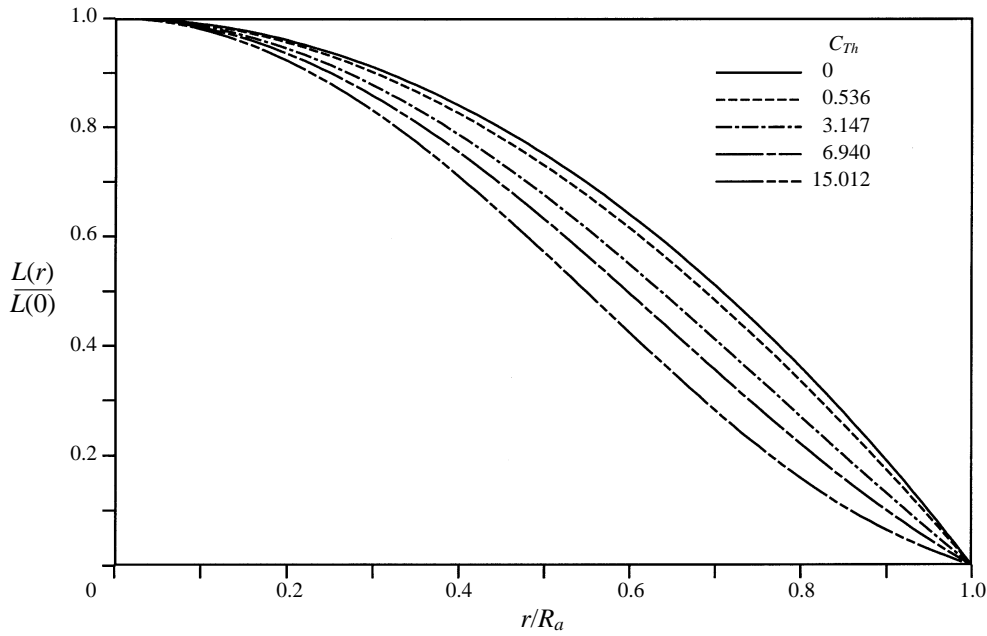
FIGURE 8. Normalized disk load distributions for various values of C_{Th}.

shooting method with two-point boundary conditions to obtain accurate values for C_{Th}, C_P and η. The conditions $\Psi = 0$ for $r = 0$ and $\mathrm{d}\Psi/\mathrm{d}r = 0$ for $\Psi = \Psi_e$ can always be used. Equation (4.4) can be solved analytically for some special cases.

An alternative representation to (4.3) which can accurately approximate an arbitrary vorticity component $\omega_\phi(r, z)$ within the slipstream for N sufficiently large is

$$\frac{\omega_\phi(r, z)}{r} = \sum_{n=0}^{N} A_n(z) \left[1 - \left(\frac{r}{R(z)} \right)^2 \right]^n. \tag{4.5}$$

The $A_n(z)$ can be expected to be only weak functions of z as ω_ϕ/r is constant along streamlines. Since the axis of symmetry and the slipstream boundary $r = R(z)$ are both streamlines, it follows that $A_0 = \mathrm{const}$ and $\sum_{n=1}^{N} A_n(z) = \mathrm{const}$. In the limit of light loading then $R(z) = R_a$ and $\Psi/\Psi_e = (r/R_a)^2$, so the relation between (4.3) and (4.5) is simple and direct, with all of the A_n constant.

If (4.5) is substituted into (2.5), (2.6) and (2.7), the radial integrations can be performed immediately using the following integral (Gradshteyn & Ryzhik 1980), which is due to Sonine (1880):

$$\int_0^1 x^{\nu+1} (1 - x^2)^\mu J_\nu(bx) \mathrm{d}x = 2^\mu \Gamma(\mu + 1) b^{-(\mu+1)} J_{\nu+\mu+1}(b). \tag{4.6}$$

The integrations with respect to s are of the form described by (3.7) and can also be performed to give the one-dimensional axial integrals

$$\Psi(r, z) = \frac{U_\infty r^2}{2} + r \int_0^\infty \sum_{n=0}^{N} A_n(z') 2^{n-1} n! R^{2-n}(z') I_{(-(n+1), n+2, 1)}(R(z'), r, z - z') \mathrm{d}z', \tag{4.7}$$

$$V_r(r,z) = \int_0^\infty \pm \sum_{n=0}^N A_n(z')2^{n-1}n!R^{2-n}(z')I_{(-n,n+2,1)}(R(z'),r,z-z')\mathrm{d}z', \qquad (4.8)$$

$$V_z(r,z) = \int_0^\infty \sum_{n=0}^N A_n(z')2^{n-1}n!R^{2-n}(z')I_{(-n,n+2,0)}(R(z'),r,z-z')\mathrm{d}z'. \qquad (4.9)$$

The above integrals provide complete solutions for the stream function and velocity components of a generalized contra-rotating propeller once the slipstream boundary $R(z)$ and the functions $A_n(z)$ have been determined iteratively. The functions $A_n(z)$ can be determined within the same iteration loop as the slipstream boundary by generalizing (3.11) to give

$$\Psi(R_a,0) = \frac{U_\infty R^2(z)}{2}$$

$$+ R(z)\int_0^\infty \sum_{n=0}^N A_n(z')2^{n-1}n!R^{2-n}(z')I_{(-(n+1),n+2,1)}(R(z'),r,z-z')\mathrm{d}z'. \quad (4.10)$$

At the ith iteration we define

$$I_i(z) = \int_0^\infty \sum_{n=0}^N A_n^i(z')2^{n-1}n!R_i^{2-n}(z')I_{(-(n+1),n+2,1)}(R_i(z'),R_i(z),z-z')\mathrm{d}z' \qquad (4.11)$$

and the iteration for the slipstream boundary is

$$R_{i+1}(z) = \left\{ \left(\frac{I_i(z)}{U_\infty}\right)^2 + \frac{2\Psi_i(R_a,0)}{U_\infty} \right\}^{1/2} - \frac{I_i(z)}{U_\infty}. \qquad (4.12)$$

For the first iteration the constant A_n values of the lightly loaded limit are used. The functions $A_n(z)$ are evaluated at each subsequent iteration by evaluating $\Psi(r,z_s)$ at a set of axial stations z_s within the slipstream and then least-squares fitting (4.5) to match (4.3). The coefficients $A_n(z)$ are then obtained at all other values of z by interpolation. For the solutions to be presented here, 11 equally spaced axial stations were specified from $z/R_a = 0$ to $z/R_a = 5$, and at each station Ψ was evaluated at 11 equally spaced points from $r/R(z) = 0$ to $r/R(z) = 1$.

In the current work, (4.2) has been used directly to specify the specific enthalpy in the slipstream. This has the advantage that $h(\Psi)$ is known *a priori* as a function of Ψ/Ψ_e and therefore (4.4) can be integrated directly to give the limiting solution at downstream infinity and hence validate the results of the full solution. The disadvantage is that the relationship in the disk plane between Ψ and the radial coordinate r is not known until after the solution has been completed, and therefore the load distribution at the disk is not directly specified as a function of r. This difficulty can be overcome by specifying $h(r,0)$ in the disk plane and updating the coefficients a_m in (4.2) to match $h(r,0)$ at each iteration.

4.1. *Results*

The simplest case of (4.3) for which the load distribution falls to zero at both root and tip is

$$h(\Psi) = h_0 + a_1\left[\frac{\Psi}{\Psi_e} - \left(\frac{\Psi}{\Psi_e}\right)^2\right]. \qquad (4.13)$$

Introducing a non-dimensional coefficient $\hat{b} = R_a^2 a_1 / U_\infty \Psi_e$ gives

$$\frac{\omega_\phi}{r} = \frac{U_\infty \hat{b}}{R_a^2} \left[2 \left(\frac{\Psi}{\Psi_e} \right) - 1 \right] \tag{4.14}$$

and in the lightly loaded limit (4.5) takes the form

$$\frac{\omega_\phi}{r} = \frac{U_\infty \hat{b}}{R_a^2} \left\{ 1 - 2 \left[1 - \left(\frac{r}{R_a} \right)^2 \right] \right\}. \tag{4.15}$$

For this special case (4.4) becomes

$$\frac{1}{r} \frac{\mathrm{d}}{\mathrm{d}r} \left(\frac{1}{r} \frac{\mathrm{d}\Psi}{\mathrm{d}r} \right) = \frac{U_\infty \hat{b}}{R_a^2} \left[1 - 2 \left(\frac{\Psi}{\Psi_e} \right) \right] \tag{4.16}$$

and the substitution $t \equiv r^2$ reduces (4.16) to the simple harmonic motion equation. For $\hat{b} > 0$ it is convenient to define a parameter $\beta \equiv (U_\infty \hat{b} / 2 R_a^2 \Psi_e)^{1/2}$ and then the solution of (4.16) subject to the conditions $\Psi(0, \infty) = 0$ and $\Psi(R_d, \infty) = \Psi_e$ becomes

$$\Psi(r, \infty) = \frac{\Psi_e}{2} \left(1 - \cos \beta r^2 + \frac{(1 + \cos \beta R_d^2) \sin \beta r^2}{\sin \beta R_d^2} \right). \tag{4.17}$$

To satisfy the condition $V_z(R_d, \infty) = 0$ we must have

$$\frac{\beta \Psi_e}{U_\infty} = \frac{\sin \beta R_d^2}{1 + \cos \beta R_d^2} \tag{4.18}$$

and therefore

$$\frac{V_z(r, \infty)}{U_\infty} = \cos \beta r^2 - 1 + \frac{\sin \beta R_d^2}{1 + \cos \beta R_d^2} \sin \beta r^2. \tag{4.19}$$

Hence the formulae analogous to (3.15), (3.16) and (3.17) are

$$C_{Th} = \frac{2}{1 + \cos \beta R_d^2} \left(\frac{R_d}{R_a} \right)^2 \left[1 - \frac{\sin \beta R_d^2}{\beta R_d^2} \right], \tag{4.20}$$

$$C_P = \frac{4}{3 \beta R_d^2} \left(\frac{R_d}{R_a} \right)^2 \left[\frac{\sin \beta R_d^2}{1 + \cos \beta R_d^2} \right]^3, \tag{4.21}$$

$$\eta = \frac{3 (\beta R_d^2 - \sin \beta R_d^2) \sin \beta R_d^2}{2 (1 - \cos \beta R_d^2)^2}. \tag{4.22}$$

Equivalent formulae can be derived in terms of hyperbolic functions for the case of a windmill where $\hat{b} < 0$. The efficiency η depends only on the dimensionless group βR_d^2 and from (4.18) this is given implicitly in terms of the mean normalized perturbation velocity $\bar{v}$ in the ultimate wake by the equation

$$1 + \bar{v} = \frac{2 \sin \beta R_d^2}{\beta R_d^2 (1 + \cos \beta R_d^2)}. \tag{4.23}$$

Figure 9 compares the efficiency $\eta(\bar{v})$ given by (4.22) and (4.23) with (3.19) and (3.18). As might be expected, the ideal efficiency η_i specified by (3.19) is the highest for given $\bar{v}$ of the three analytical formulae shown. However, the efficiency η given by (4.22) and (4.23), which corresponds to a case for which both the load distribution and $h - h_0$ vanishes both at $r = 0$ and $r = R_a$, is higher at given $\bar{v}$ than for (3.18), for
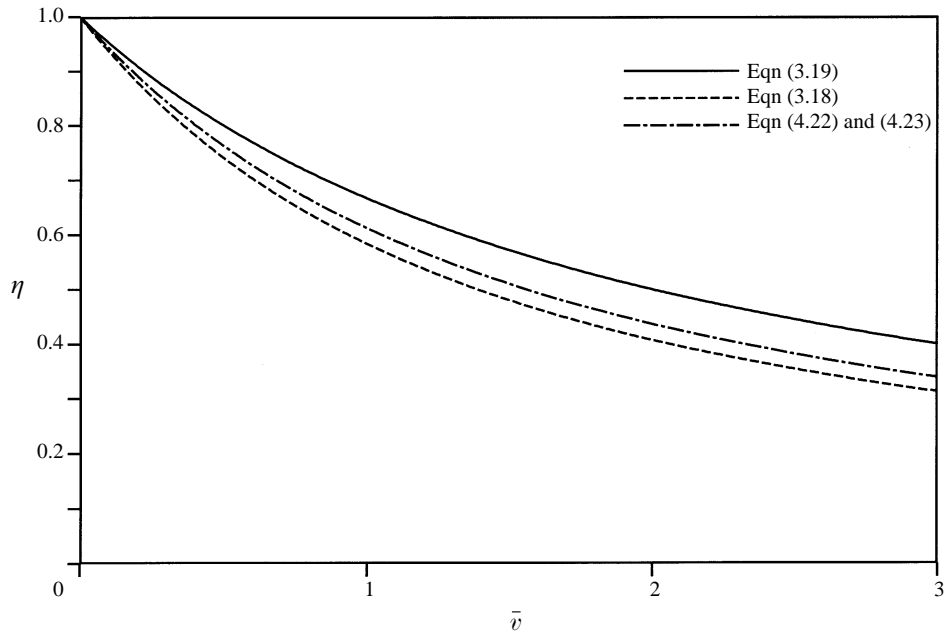
FIGURE 9. Efficiency $\eta(\bar{v})$ given by various analytical expressions.

which the load distribution and $h - h_0$ vanish only at $r = R_a$. Figure 10 compares the numerically computed efficiencies for these two cases as a function of the thrust coefficient C_{Th}. At specified thrust coefficient, the case with the enthalpy determined by (4.13) again gives higher efficiency than when the enthalpy is determined by (3.1), though both efficiency curves are quite close despite the differences in the underlying load distributions. It is shown below that despite the simplicity of (4.13), it gives rise to a load distribution representative of a generic propeller. Hence the inviscid efficiency of a real propeller can be expected to be represented more accurately by (4.22) and (4.23) than by the ideal efficiency given by (3.19).

Figure 11 shows the converged slipstream boundaries for various values of $\hat{b}$, and these contractions are qualitatively similar to those given in figure 2. Figure 12 shows the corresponding disk load distributions. Despite the simplicity of (4.13), these are remarkably good representations of generic propeller radial distributions. Figure 13 gives the radial velocity distribution in the disk plane and at various axial stations fore and aft of the disk for $\hat{b} = 5$, which corresponds to $C_{Th} = 0.9533$ and $\eta = 0.8099$. These distributions qualitatively resemble the corresponding distributions obtained by Conway (1995) for a linearized disk with hub, apart from the discontinuity in $\partial V_r / \partial r$ at $r = R(z)$, and the breaking of the fore/aft symmetry.

Figure 14 shows the induced axial velocities for $\hat{b} = 5$ at the disk and at different axial stations fore and aft of the disk. A notable feature is that although the load distribution vanishes at $r = 0$ for this case and therefore the velocity along the axis vanishes in the linear limit, the nonlinear axial perturbation velocity $V_z(r, 0)/U_\infty$ does not vanish on the axis, and is substantially negative. This negative perturbation velocity near the axis results because the boundary condition of zero load at the axis has been imposed, making $\mathrm{d}h/\mathrm{d}\Psi$ positive near the axis and of course negative near the disk rim. From (2.17) it can be seen that ω_ϕ is therefore necessarily opposite in sign in the inner part of the slipstream to its value in the much larger outer region of
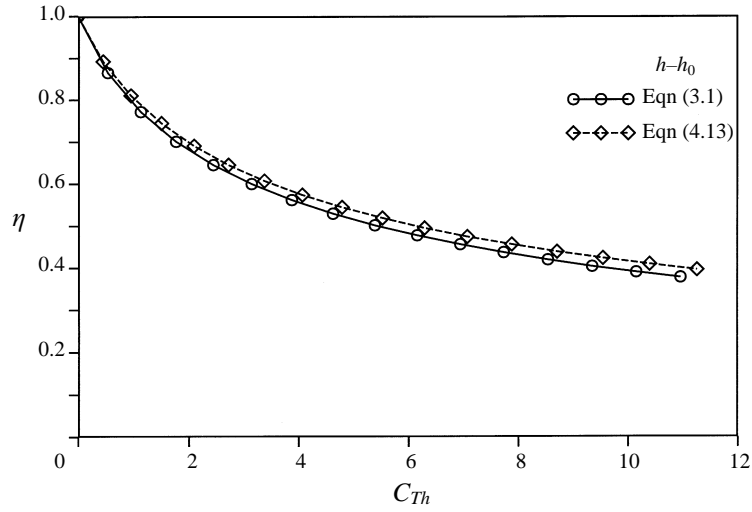
J. T. Conway

FIGURE 10. Computed efficiency $\eta(C_{Th})$ for enthalpy determined by (3.1) and (4.13). The symbols give the computed points.
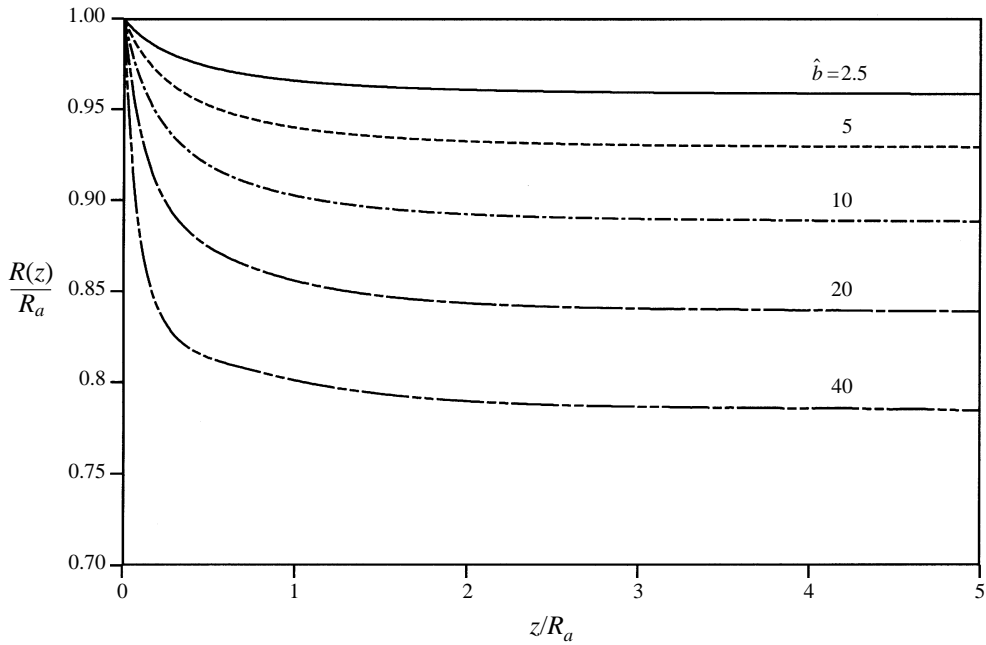

FIGURE 11. Converged slipstream boundaries for various values of $\hat{b}$.

the slipstream. The velocity field induced by the ring vortex distribution in the inner part of the slipstream will therefore be opposite in direction to that induced by the distribution in the outer part. The relative strengths of these competing inductions can in general only be calculated by nonlinear calculations such as those presented here, though competing trends can sometimes be qualitatively understood. This is illustrated by figure 15, which shows the normalized induced axial velocity along the axis of symmetry for various values of the thrust coefficient C_{Th}. Far upstream of
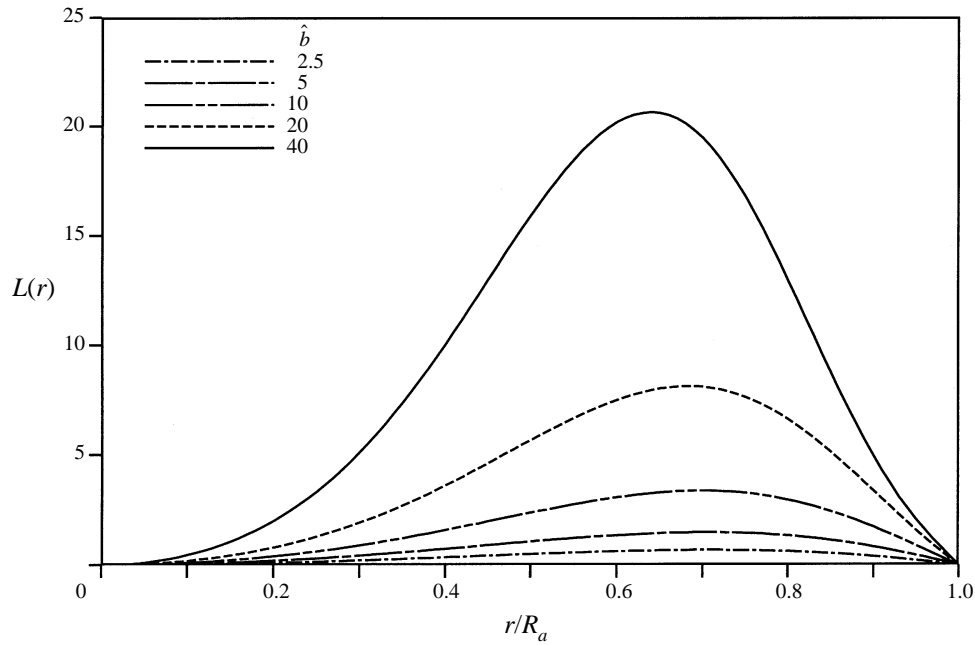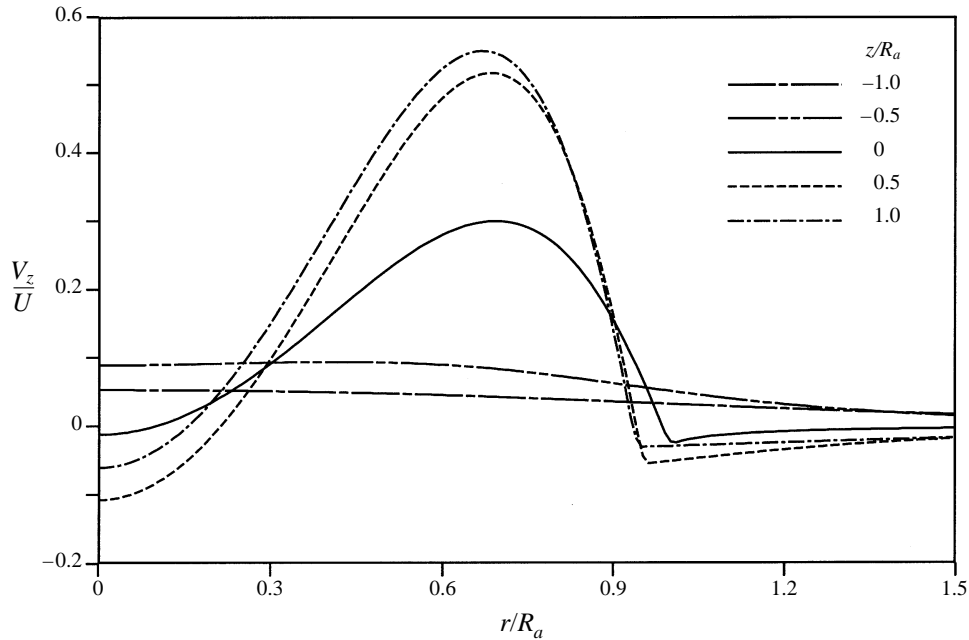
FIGURE 12. Disk load distributions for varous values of $\hat{b}$.
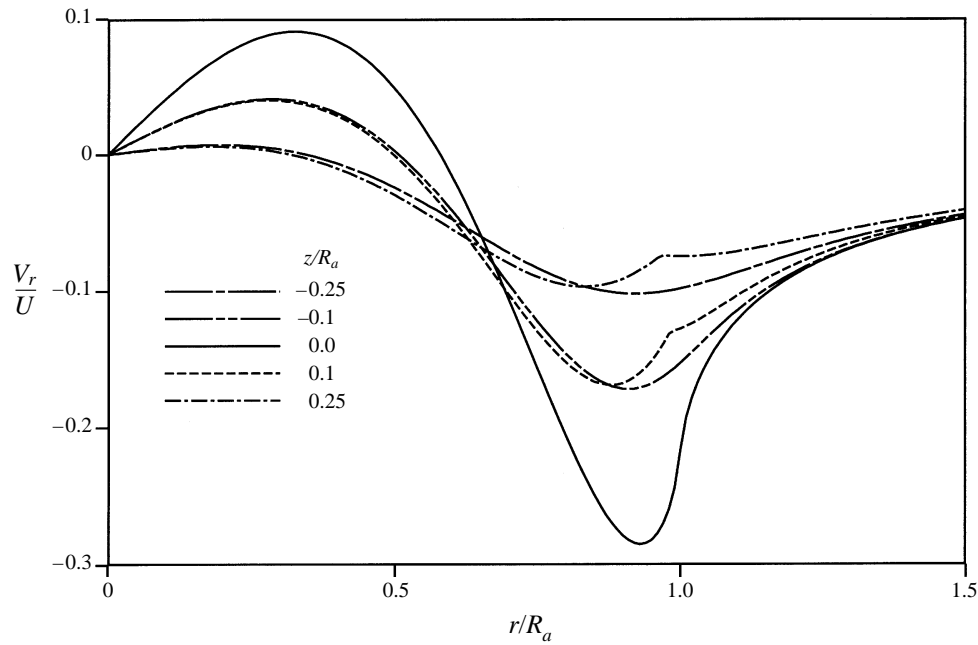
FIGURE 13. Radial velocity distribution $V_r(r, z)$ for various values of the axial coordinate z for $\hat{b} = 5$.

the disk, the induced axial velocity is positive. This is because the ring vortices in the outer part of the slipstream are of greater physical dimensions than those in the inner region, so their induction effect falls off less rapidly with distance and they dominate upstream of the disk. However near the disk and downstream of it, the inner ring

FIGURE 14. Induced axial velocity distributions $V_z(r, z)$ for various values of the axial coordinate z for $\hat{b} = 5$.

vortices dominate due to their closer proximity to the axis and the total induced axial velocity is negative. Application of the Bernoulli equation along the axis shows that the axial induction must necessarily vanish in the limit of downstream infinity, as can be seen in figure 15.

Figure 16 shows the approach of the axial velocity profile calculated by the general method to the analytical formula (4.19) for the downstream limiting profile. At two propeller diameters downstream of the disk, the velocity profile has almost achieved its limiting asymptotic form. This provides very strong verification of the numerics of the general calculation scheme.

5. Propellers with slipstream rotation

It is straightforward to generalize the results obtained so far to the case of propellers with swirl. Substituting (2.31) into (2.33) gives

$$\frac{\omega_\phi}{r} = \left(\frac{h - h_0}{(\Omega r)^2} - 1 \right) \frac{\mathrm{d}h}{\mathrm{d}\Psi}. \tag{5.1}$$

Equation (2.17) is recovered from (5.1) in the case where $\Omega \to \infty$. This result may appear counter-intuitive, but is a consequence of the fact that the circulation Γ along the blades must vanish if the load distribution along the blades is held finite as $\Omega \to \infty$. It follows from vorticity conservation that the longitudinal vorticity components ω_z and ω_r must also vanish and therefore from Stokes's theorem the swirl component V_ϕ must also vanish in the slipstream.

For finite Ω, the azimuthal velocity component $V_\phi(r, z)$ is given from (2.31) by
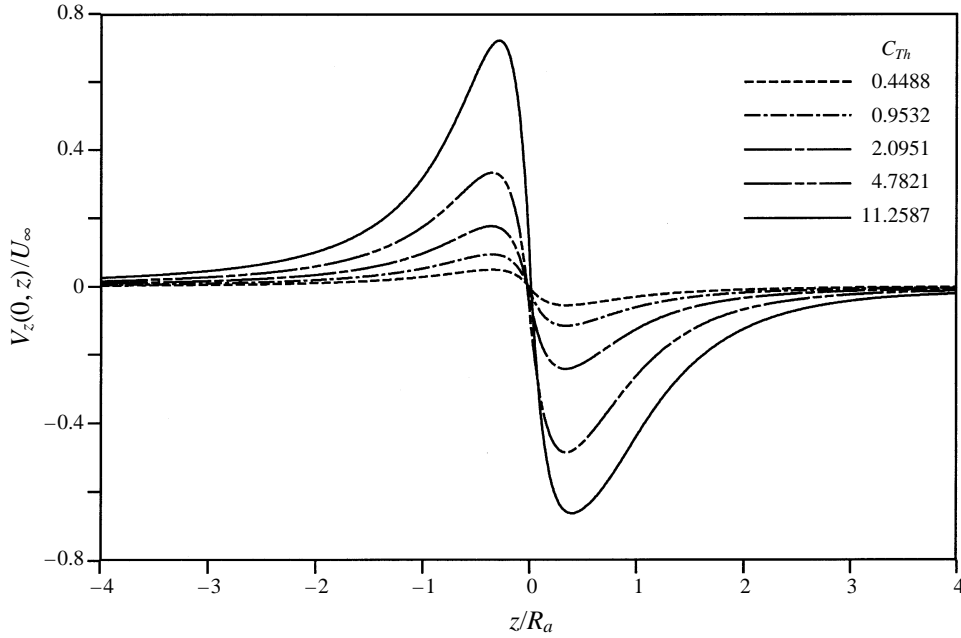
$$V_\phi(r, z) = \frac{h - h_0}{\Omega r}, \tag{5.2}$$

FIGURE 15. Normalized axial velocity $V_z(0,z)/U_\infty$ along the axis of symmetry for various values of the thrust coefficient C_{Th}.

and therefore, unlike the contra-rotating case, when slipstream rotation is present the load distribution must fall to zero at the blade roots to avoid singular behaviour, unless a finite hub is introduced. As before, the specific enthalpy in the slipstream can be represented by (4.2), and ω_ϕ is given by (4.5) everywhere in the slipstream. From (2.29) and (3.23) the propeller load distribution is given by

$$L(r) = \frac{h(\Psi(r,0)) - h_0}{U_\infty^2} \left(2 - \frac{h(\Psi(r,0)) - h_0}{(\Omega r)^2} \right). \tag{5.3}$$

If we again choose the simplest case where the specific enthalpy is given by (4.13), then from (5.1) the vorticity in the slipstream is given by

$$\frac{\omega_\phi}{r} = \frac{U_\infty \hat{b}}{R_a^2} \left[2 \left(\frac{\Psi}{\Psi_e} \right) - 1 \right] \left[1 - \frac{\hat{b}J^2}{\pi^2} \left(\frac{\Psi_e}{U_\infty r^2} \right) \left(\frac{\Psi}{\Psi_e} - \left(\frac{\Psi}{\Psi_e} \right)^2 \right) \right], \tag{5.4}$$

which on the axis of symmetry reduces to

$$\frac{\omega_\phi}{r} = \frac{U_\infty \hat{b}}{R_a^2} \left[\frac{\hat{b}J^2}{2\pi^2} \left(1 + \frac{V_z}{U_\infty} \right) - 1 \right] \tag{5.5}$$

and in the lightly loaded limit reduces to

$$\frac{\omega_\phi}{r} = \frac{U_\infty \hat{b}}{R_a^2} \left\{ 1 - 2 \left[1 - \left(\frac{r}{R_a} \right)^2 \right] \right\} \left\{ 1 - \frac{\hat{b}J^2}{2\pi^2} \left[1 - \left(\frac{r}{R_a} \right)^2 \right] \right\}, \tag{5.6}$$

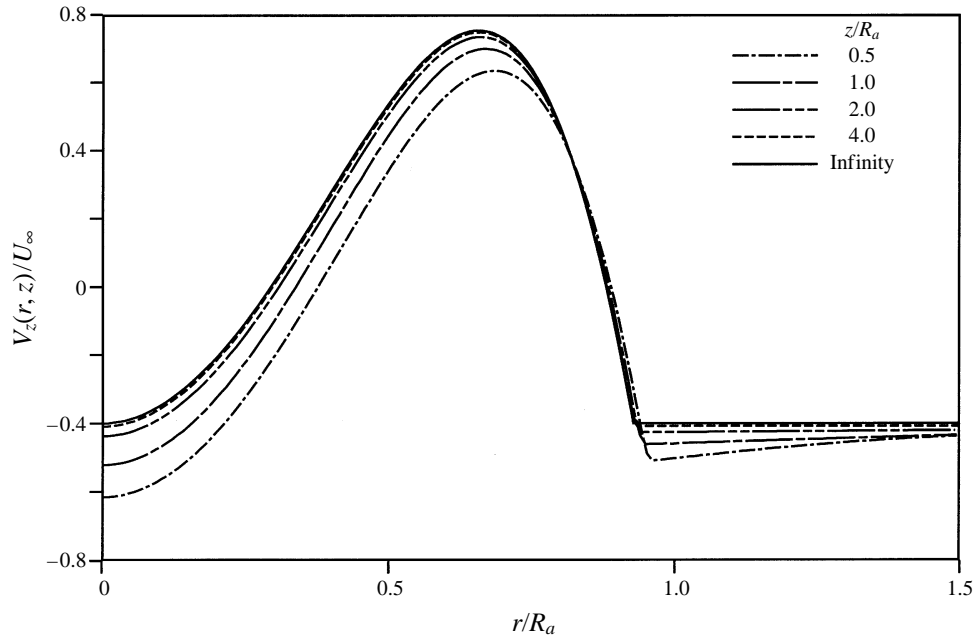where $J = U_\infty/nd$ is the propeller advance ratio and $d \equiv 2R_a$ is the propeller diameter.

FIGURE 16. Approach of the Induced axial velocity $V_z(r,z)$ for $\hat{b} = 5$ to the analytical formula (4.19) for the downstream limit.

In the downstream limit (5.4) gives the ordinary differential equation

$$\frac{1}{r}\frac{\mathrm{d}}{\mathrm{d}r}\left[\frac{1}{r}\frac{\mathrm{d}}{\mathrm{d}r}\left(\frac{\Psi}{\Psi_e}\right)\right] = \frac{U_\infty \hat{b}}{R_a^2 \Psi_e}\left[1 - 2\left(\frac{\Psi}{\Psi_e}\right)\right]\left[1 - \frac{\hat{b}J^2}{\pi^2}\left(\frac{\Psi_e}{U_\infty r^2}\right)\left(\frac{\Psi}{\Psi_e} - \left(\frac{\Psi}{\Psi_e}\right)^2\right)\right],$$

$$(5.7)$$

which can be numerically integrated, subject to the two-point boundary conditions $\Psi = 0$ at $r = 0$ and $\mathrm{d}\Psi/\mathrm{d}r = 0$ when $\Psi = \Psi_e$ at the slipstream boundary, to give an accurate solution at downstream infinity once a value for Ψ_e has been obtained from the iterative solution of (4.10). Here a standard Runge–Kutta solver from the book by Press *et al.* (1992) was used.

From (4.13) and (5.2) the azimuthal velocity in the slipstream is given by

$$\frac{V_\phi(r,z)}{U_\infty} = \frac{\hat{b}J\Psi_e}{\pi R_a U_\infty r}\left[\frac{\Psi}{\Psi_e} - \left(\frac{\Psi}{\Psi_e}\right)^2\right],$$

$$(5.8)$$

which in the lightly loaded limit reduces to

$$\frac{V_\phi(r,z)}{U_\infty} = \frac{\hat{b}Jr}{2\pi R_a}\left[1 - \left(\frac{r}{R_a}\right)^2\right].$$

$$(5.9)$$

In a propeller slipstream with rotation, the pressure in the ultimate wake is not equal to the free-stream pressure except at the slipstream boundary, and (3.13) and (3.14) must be modified to take this into account. By calculating the flow of momentum and energy in and out of a suitable control volume in the limit as the dimensions of the volume become infinite, it is straightforward to show that (3.13) and (3.14) generalize

to give

$$T = 2\pi\rho \int_0^{Rd} \left\{ \frac{p - p_\infty}{\rho} + U_\infty V_z(r, \infty) + V_z^2(r, \infty) \right\} r\, dr \qquad (5.10)$$

which can be written as

$$T = 2\pi\rho \int_0^{Rd} \left\{ h - h_0 + \frac{V_z^2(r, \infty) - V_\phi^2(r, \infty)}{2} \right\} r\, dr, \qquad (5.11)$$

and

$$P = 2\pi\rho \int_0^{Rd} (U_\infty + V_z(r, \infty))(h - h_0) r\, dr. \qquad (5.12)$$

Equation (5.12) can also be obtained very simply by equating the propeller torque Q to the rate of generation of angular momentum in the slipstream and employing (2.31) and the relation $P = \Omega Q$. From (5.11), (5.12) and (2.31), C_{Th} and C_P are given by

$$C_{Th} = \frac{4}{R_a^2} \int_0^{Rd} \left\{ \frac{\pi r}{JR_a} \left(\frac{V_\phi(r, \infty)}{U_\infty} \right) + \frac{1}{2} \left[\left(\frac{V_z(r, \infty)}{U_\infty} \right)^2 - \left(\frac{V_\phi(r, \infty)}{U_\infty} \right)^2 \right] \right\} r\, dr \qquad (5.13)$$

and

$$C_P = \frac{4\pi}{JR_a^3} \int_0^{Rd} \left(1 + \frac{V_z(r, \infty)}{U_\infty} \right) \frac{V_\phi(r, \infty)}{U_\infty} r^2\, dr. \qquad (5.14)$$

Equations (5.13) and (5.14) can be integrated numerically to obtain accurate values for C_{Th}, C_P and η from the solution at downstream infinity, and it is straightforward to evaluate these integrals within the Runge–Kutta solution for the velocities. Equation (5.12) is in a form which can be directly integrated analytically for the general case using (4.2) which gives

$$C_P = \frac{4\Psi_e}{U_\infty^3 R_a^2} \sum_{m=0}^{M} \frac{a_m}{m + 1}. \qquad (5.15)$$

5.1. *Results*

Figure 17 shows the convergence (without under-relaxation) of the slipstream boundary for the case where $\hat{b} = 5$ and $J = 1$, which corresponds to a slipstream contraction $R_d/R_a = 0.9293$, almost identical to that with the same value of $\hat{b}$ without slipstream rotation. For this case $\Psi_e/U_\infty R_a^2 = 0.5959$, $C_{Th} = 0.8903$, $C_P = 1.184$ and the efficiency $\eta = 0.7521$. No noticeable effects of advance ratio J on the convergence of the iteration for the slipstream boundary were found. Figure 18 shows the streamline pattern for a more heavily loaded case with $\hat{b} = 15$ and $J = 1$. For this case $C_{Th} = 2.510$, $C_P = 5.971$ and the efficiency $\eta = 0.4203$. The streamlines pass through the actuator disk smoothly, crossing it only once, and no particular problems occur near the disk rim.

Figure 19 shows the disk load distribution $L(r)$ as defined by (3.23) for $\hat{b} = 5$ and various values of the advance ratio J. These distributions are reasonably representative of load distributions for a generic propeller. For fixed $\hat{b}$ the maximum of the distribution moves outwards toward the rim as the advance ratio increases. There is a substantial decrease in C_{Th} with increasing J, and this occurs at almost constant mass flow through the disk, as Ψ_e increases by less than 1% from $J = 0$ to $J = 2$. Figure 20 shows the various non-dimensional coefficients as a function of
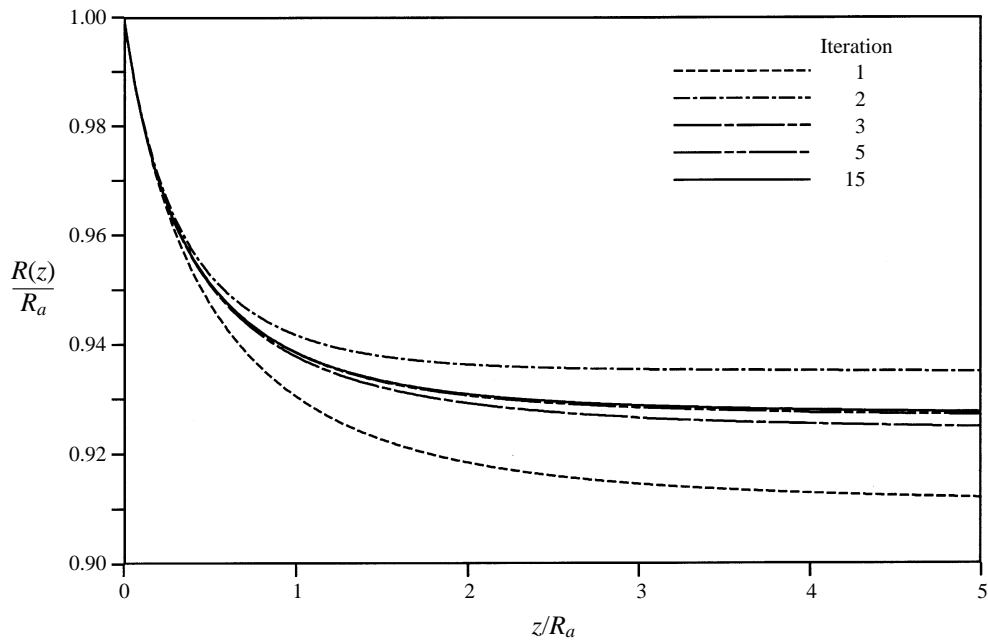
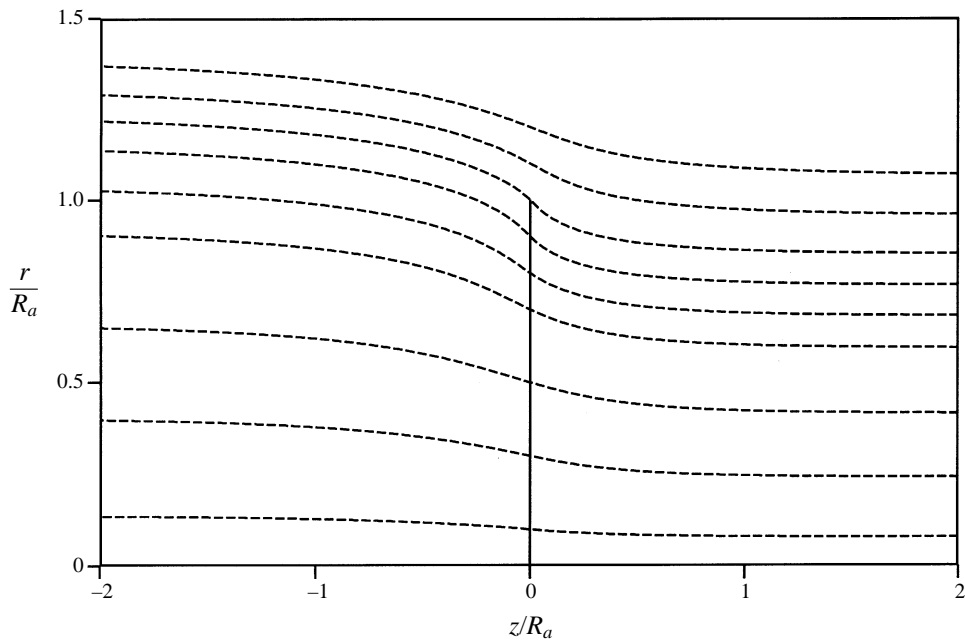FIGURE 17. Convergence of the slipstream boundary for $\hat{b} = 5$ and $J = 1$.

FIGURE 18. Streamlines for a more heavily loaded case with $\hat{b} = 15$ and $J = 1$.

J for this value of $\hat{b}$. The propeller efficiency falls with J for fixed $\hat{b}$, almost entirely to the reduction in the thrust coefficient, as the power coefficient C_P increases only slightly with increasing J.

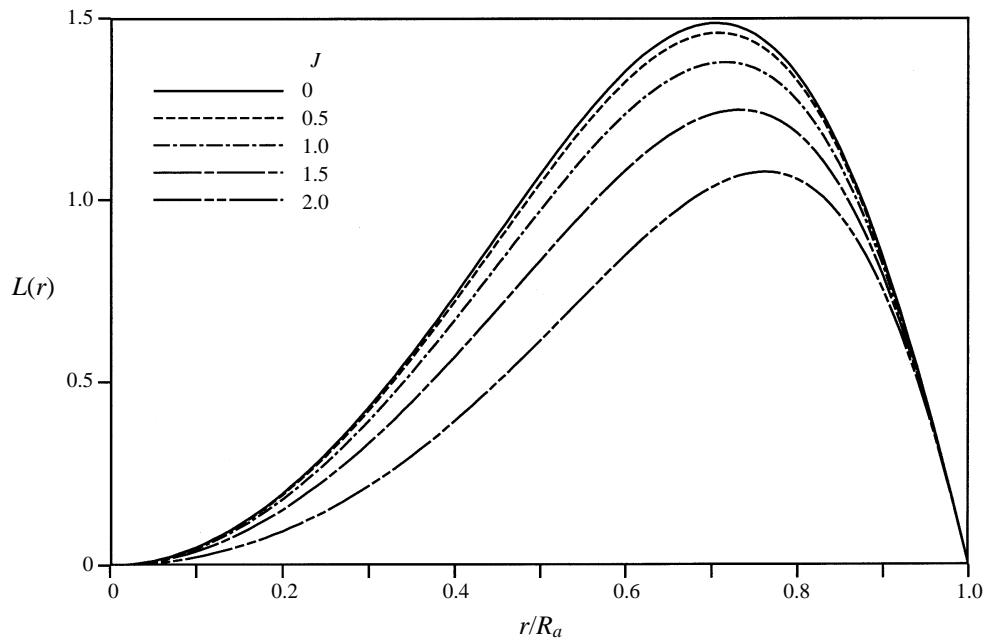Figure 21 shows the radial variation of the axial perturbation velocity at various

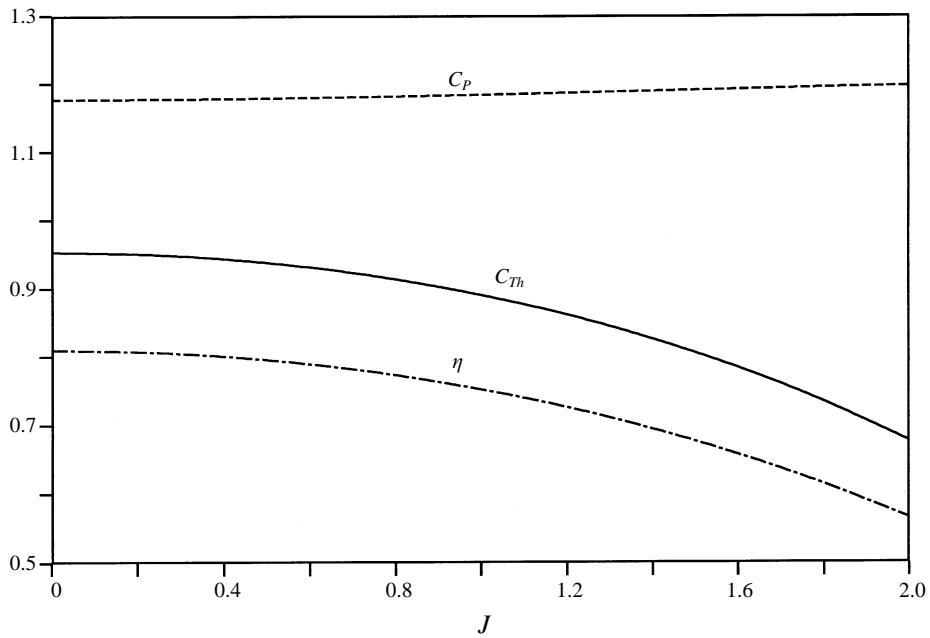FIGURE 19. Disk load distribution for $\hat{b} = 5$ and various values of the advance ratio J.

FIGURE 20. Non-dimensional coefficients as functions of the advance ratio J.

axial stations fore and aft of the disk for $\hat{b} = 5$ and $J = 1$. In contrast to the results for $J = 0$, the axial perturbation velocity $V_z(0, z)$ does not vanish in the downstream limit, even though the disk load distribution falls to zero at the axis for this case. That this should be so can be seen from elementary considerations. The pressure at the slipstream boundary in the downstream limit must equal the free-stream pressure,
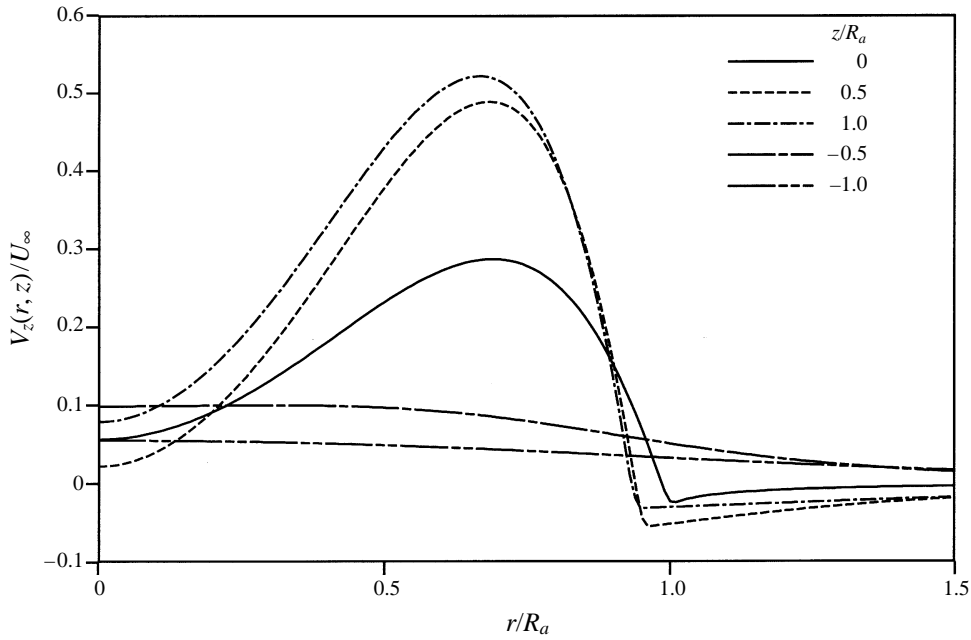
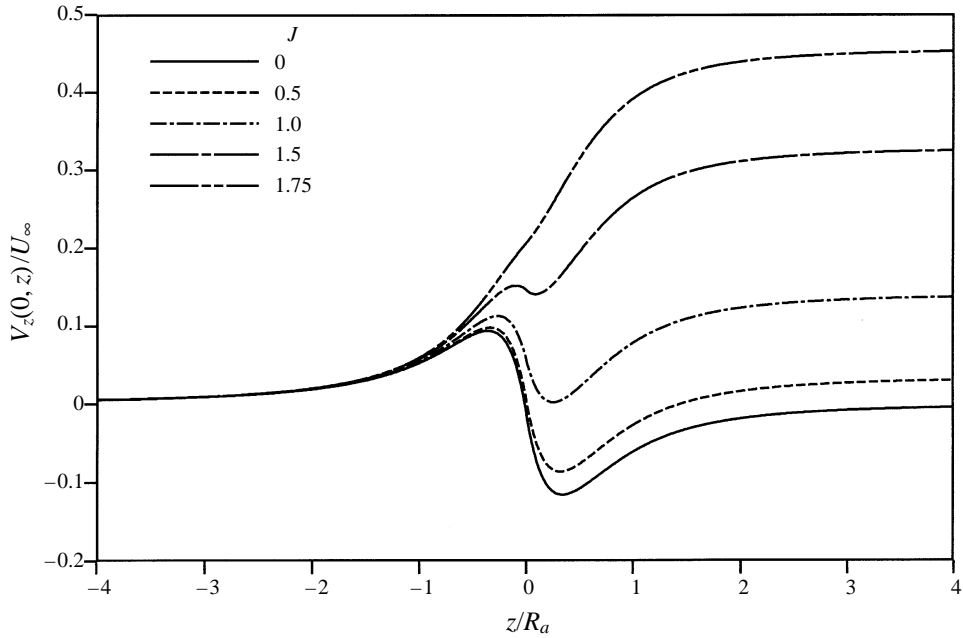FIGURE 21. $V_z(r,z)$ at axial stations fore and aft of the disk for $\hat{b} = 5$ and $J = 1$.

FIGURE 22. $V_z(0,z)$ along the axis of symmetry for $\hat{b} = 5$ and various values of the advance ratio J.

and must fall monotonically within the slipstream to provide the pressure gradient which maintains the fluid particles in spiral paths of constant radius. Therefore the pressure along the axis of symmetry in the downstream limit is below free-stream and decreases with increasing advance number J. The Bernoulli equation can again be applied along the entire axis of symmetry and as V_z is the only perturbation velocity
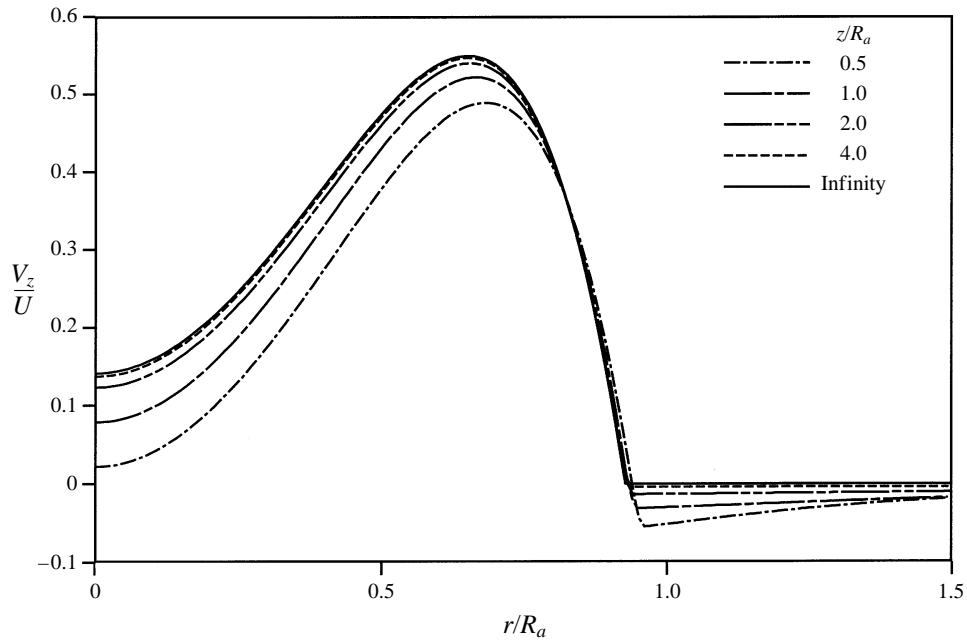
FIGURE 23. Approach of the axial velocity profile to the asymptotic limiting profile.
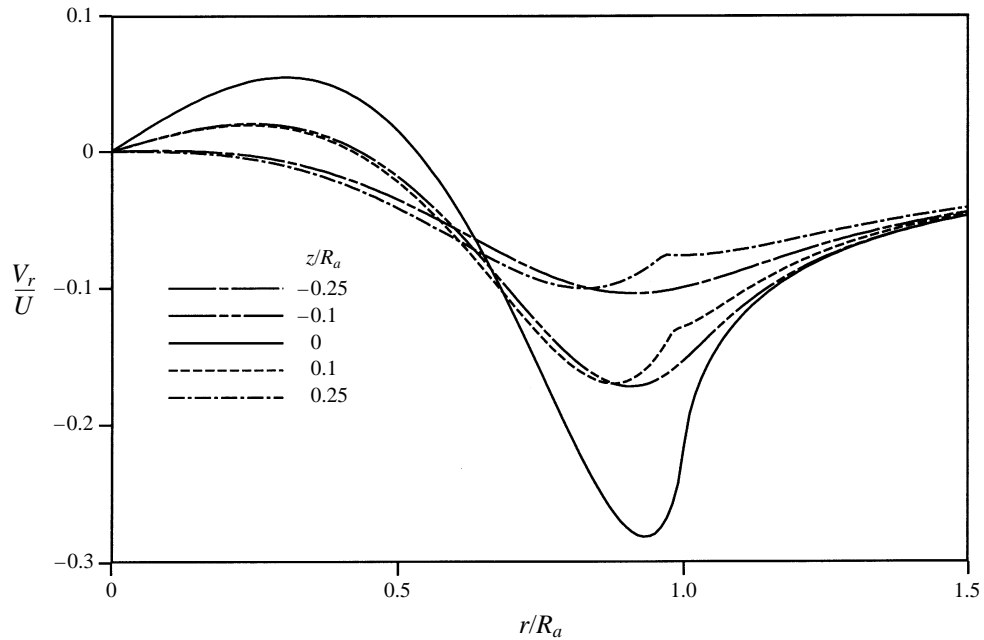

FIGURE 24. Radial velocity distributions in the disk plane and at axial stations fore and aft of the disk for $\hat{b} = 5$ and $J = 1$.

component which is not necessarily zero, it follows that $V_z(0, z)$ does not tend to zero in the downstream limit. Figure 22 shows $V_z(0, z)$ along the axis of symmetry for $\hat{b} = 5$ and various values of the advance ratio J. For moderate values of J, $V_z(0, z)$ has a local minimum a short distance downstream of the disk. The principal difference
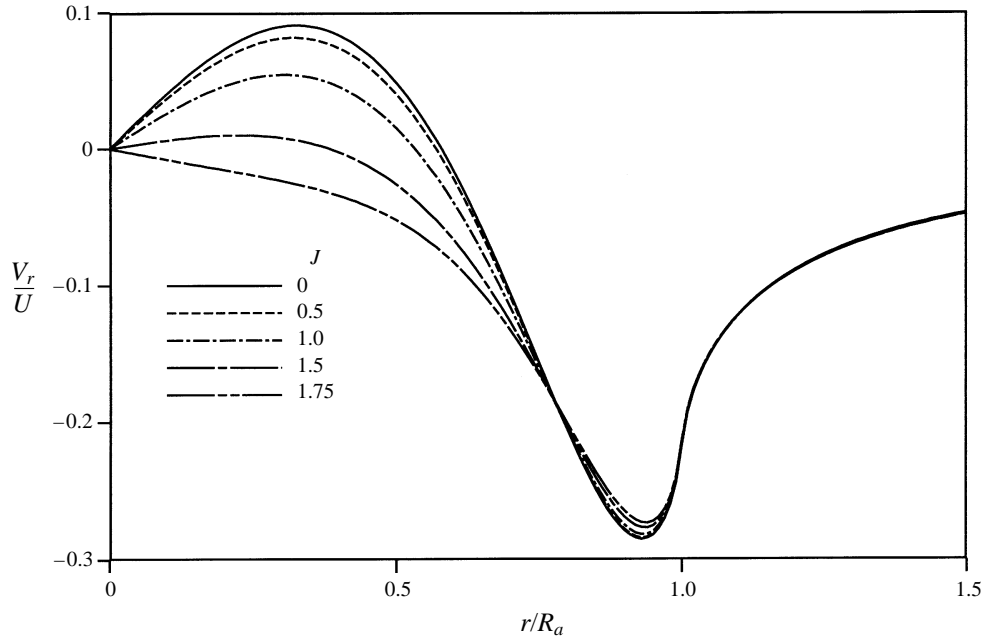
FIGURE 25. Effect of advance ratio on the radial velocity profile at the disk for $\hat{b} = 5$.
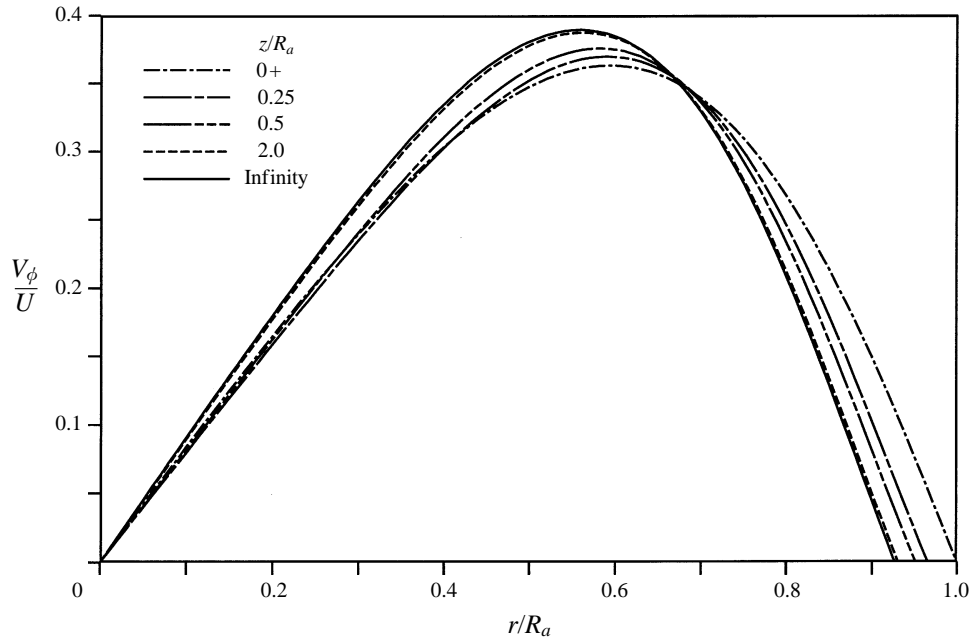

FIGURE 26. Azimuthal velocity V_ϕ for $\hat{b} = 5$ and $J = 1$ at various axial stations downstream of the disk.

between figure 21 and figure 16 is that $V_z(0,0)$ is positive rather than negative. This is qualitatively understandable from inspection of figure 22, where it can be seen that the suction produced by the low pressure along the axis at downstream infinity alters the balance between the competing inductions progressively in favour of positive induced $V_z(0,z)$ as the advance ratio and hence the swirl in the slipstream is increased.

The approach of $V_z(r, z)$ as z increases to the asymptotic profile $V_z(r, \infty)$ calculated by the Runge–Kutta shooting method is shown in figure 23 for $\hat{b} = 5$ and $J = 1$. By two propeller diameters downstream of the disk, the difference between the velocity profile and its asymptotic limit is very small.

Figure 24 gives the radial velocity $V_r(r, z_s)$ in the disk plane and at various axial stations z_s fore and aft of the disk for $\hat{b} = 5$ and $J = 1$. The radial profiles are qualitatively similar to those given in figure 13 for $J = 0$. The effect of advance ratio on V_r is shown in figure 25, which gives $V_r(r, 0)$ for $\hat{b} = 5$ and various values of the advance ratio J. The effect of J on the radial velocity profile at the disk is considerable, falls towards the slipstream boundary, and is negligible outside the slipstream where the azimuthal velocity V_ϕ is zero.

Finally, figure 26 shows the azimuthal velocity $V_\phi(r, z_s)$ at various axial stations z_s downstream of the disk and the asymptotic profile at $z_s = \infty$, for $b = 5$, $C_{Th} = 0.8903$ and $J = 1$. The variation of the V_ϕ profile with axial position within the slipstream is of course much less than for the other induced velocities. $V_\phi(r, z)$ is comparable in magnitude with the free-stream velocity throughout most of the slipstream for these values of C_{Th} and J, which are not unreasonable for a marine propeller.

6. Comments and conclusions

An exact method of solving for the flow induced by a heavily loaded propeller actuator disk with slipstream rotation and non-uniform loading has been developed. The method extends the linearized solution given by Conway (1995) to the heavily loaded case with slipstream contraction subject to the restriction that the radial gradient of the load, and hence the azimuthal component of the vorticity in the slipstream, is bounded. The slipstream boundary is obtained by iterative solution of a nonlinear non-singular integral equation, and the flow field is given by numerical evaluation of one-dimensional integrals containing elliptic integral expressions similar to those which occur in the linearized solution. The propeller efficiency, thrust, torque and flow field can be calculated for any realistic load distribution with bounded radial gradient.

Results have been presented for both contra-rotating and normal propellers with realistic generic load distributions and also for a special contra-rotating case for which the vorticity distribution is known *a priori* in the slipstream and is equal to that within the well-known spherical vortex of Hill (1894). Indeed it can be shown that the spherical vortex itself is a special analytical solution of equation (3.11). It seems therefore at least a possibility that a fully analytical solution could be obtained for the slipstream boundary for this special case.

Analytical expressions for thrust, torque, efficiency and the velocities in the ultimate wake have been derived for some special cases. The full three-dimensional calculations have been validated by comparison with Runge–Kutta and analytical solutions in the ultimate wake for which the solution becomes one-dimensional.

It has been found that the fore–aft symmetry of the induced radial velocity is broken in the nonlinear case, and there is a discontinuity in the slope of the radial velocity across the slipstream boundary which is not present in the linearized case. As was found by Conway (1995) for the linearized disk, the radial velocity in the disk plane for the heavily loaded disk is comparable in magnitude to the induced axial velocity.

For the heavily loaded disk substantial deviations were found from Froude's (1889) law for the axial velocity, which is the basis of the well-known Glauert (1926, 1935) approach for the actuator disk.

The method presented here can be combined with blade element theory to provide calculations of propeller efficiency as a function of advance ratio for given propeller geometry. The method could also be embedded in a suitable panel method to calculate the effect of the propeller on its vehicle.

It remains to be seen if it is theoretically or practically possible to extend the method to encompass load distributions with a square-root or other singularity in the radial gradient at the blade tips. The method presented here can definitely not be applied to the classical special case of uniform loading, for which the slipstream boundary is a free vortex sheet. The case of bollard conditions for which $C_{Th} = \infty$ also gives difficulties as the convergence of the iteration used to solve (3.11) degrades with increasing C_{Th}, and for sufficiently high C_{Th} the axial velocity induced near the disk rim will be large enough to cause an outflow near the rim, violating the basic assumptions of actuator disk theory. However, no difficulties were experienced in obtaining solutions throughout the ranges of C_{Th} and J applicable to practical propellers.

Appendix. Solution of the integral equation

Equation (3.11) is

$$\Psi(R_a, 0) = \frac{U_\infty R^2(z)}{2} + \frac{aR(z)}{2} \int_0^\infty R^2(z') I_{(-1,2,1)}\left(R(z'), R(z), z - z'\right) dz'. \quad (A\,1)$$

This equation for the slipstream boundary $R(z)$ can be solved iteratively. If we define

$$I(z, R(z)) = \int_0^\infty R^2(z') I_{(-1,2,1)}\left(R(z'), R(z), z - z'\right) dz' \quad (A\,2)$$

then

$$R(z) = \left\{\left(\frac{aI(z, R(z))}{2U_\infty}\right)^2 + \frac{2\Psi(R_a, 0)}{U_\infty}\right\}^{1/2} - \frac{aI(z, R(z))}{2U_\infty}, \quad (A\,3)$$

and a suitable iteration scheme is

$$R_{i+1}(z) = \left\{\left(\frac{aI(z, R_i(z))}{2U_\infty}\right)^2 + \frac{2\Psi_i(R_a, 0)}{U_\infty}\right\}^{1/2} - \frac{aI(z, R_i(z))}{2U_\infty}. \quad (A\,4)$$

The first iteration can be performed analytically. Taking $R_1(z) = R_a$ where R_a is the radius of the actuator disk and defining $k \equiv 2R_a/(z^2 + 4R_a^2)^{1/2}$ gives

$$I(z, R_1(z)) = \frac{R_a^3}{8} - \frac{z^2 R_a}{4} + \frac{z}{6\pi k}\left(z^2(K(k) - E(k)) + 4R_a^2 E(k)\right). \quad (A\,5)$$

A second iteration can be obtained by substituting (A 5) into (A 4) and performing the integration in (A 2) numerically. To perform further iterations it is convenient to represent $R(z)$ in terms of a set of basis functions. The basis adopted here is the same as that used by Greenberg & Powers (1970), which represents $R(z)$ by a series of the form

$$R(z) = R_a + \sum_{n=1}^N a_n(1 - e^{-nz}). \quad (A\,6)$$

After each iteration a new representation of $R(z)$ is obtained by a least-squares fit at the discrete points at which $R(z)$ was evaluated in the previous iteration. For the results presented here 501 equally spaced points from $z/R_a = 0$ to $z/R_a = 5$ were used, though no discernible difference in the results is found if the number of points is reduced to 51.

REFERENCES

BASSET, A. B. 1888 *A Treatise on Hydrodynamics*, vol. II. Deighton Bell.

BATCHELOR, G. K. 1967 *An Introduction to Fluid Dynamics*. Cambridge University Press.

BRAGG, S. L. & HAWTHORNE, W. R. 1950 Some exact solutions of the flow through annular cascade actuator discs. *J. Aero Sci.* **17**, 243.

BRESLIN, J. P. & ANDERSEN, P. 1994 *Hydrodynamics of Ship Propellers*. Cambridge University Press.

CONWAY, J. T. 1995 Analytical solutions for the actuator disk with variable radial distribution of load. *J. Fluid Mech.* **297**, 327.

FORSYTHE, G. E., MALCOLM, M. A. & MOLER, C. 1977 *Computer Methods for Mathematical Computations*. Prentice-Hall.

FRAENKEL, L. E. 1970 On steady vortex rings of small cross-section in an ideal fluid. *Proc. R. Soc. Lond.* A **316**, 29.

FRAENKEL, L. E. 1972 Examples of steady vortex rings of small cross-section in an ideal fluid. *J. Fluid Mech.* **51**, 119.

FROUDE, R. E. 1889 On the part played in propulsion by differences in fluid pressure. *Trans. Inst. Nav. Arch.* **30**, 390.

GLAUERT, H. 1926 *The Elements of Aerofoil and Airscrew Theory*. Cambridge University Press.

GLAUERT, H. 1935 *Aerodynamic Theory*, Vol. 4 (ed. W. F. Durand). Guggenheim Fund for the Promotion of Aeronautics.

GRADSHTEYN, I. S. & RYZHIK, I. M. 1980 *Tables of Integrals, Series and Products*. Academic.

GREENBERG, M. D. 1972 Nonlinear actuator disk theory. *Z. Flugwiss.* **20**, 3, 90.

GREENBERG, M. D. & POWERS, S. R. 1970 Nonlinear actuator disk theory and flow field calculations, including nonuniform loading. *NASA Rep.* CR-1672.

HILL, M. J. M. 1894 On a spherical vortex. *Phil. Trans. R. Soc. Lond.* A **185**, 213.

HORLOCK, J. H. 1978 *Actuator Disk Theory*. McGraw Hill.

HOUGH, G. R. & ORDWAY, D. E. 1965 *Developments in Theoretical and Applied Mechanics*, vol. 2, pp. 317–336. Pergamon.

KADEN, H. 1931 Aufwicklung einer unstabilen Unstetigkeitsfläche. I*ng. Arch.* **2**, 140.

KUIK, G. A. M. VAN 1991 On the revision of the actuator disc momentum theory. *Wind Engng.* **15**, 5, 276.

LAMB, H. 1932 *Hydrodynamics*. Cambridge University Press.

NORBURY, J. 1973 A family of steady vortex rings. *J. Fluid Mech.* **57**, 417.

PRESS, W. H., TEUKOLSKI, S. A., VETTERLING, W. T. & FLANNERY, B. P. 1992 *Numerical Recipes in FORTRAN*. Cambridge University Press.

PRUDNIKOV, A. P., BRYCHKOV, Y. A. & MARICHEV, O. I. 1992 *Integrals and Series, Vol. 4: Direct Laplace Transforms*. Gordon & Breach.

PULLIN, D. I. 1978 The large-scale structure of unsteady self-similar rolled-up vortex sheets. *J. Fluid. Mech.* **88**, 401.

RANKINE, W. J. 1865 On the mechanical principles of the action of propellers. *Trans. Inst. Nav. Arch.* **6**, 13.

SCHMIDT, G. H. & SPARENBERG, J. A. 1977 On the edge singularity of an actuator disk with large constant normal load. *J. Ship Res.* **21**, 2, 125.

SONINE, N. J. 1880 Recherches sur les fonctions cylindriques et le développement des fonctions continues en séries. *Math. Ann.* **16**, 1.

THWAITES, B. (Ed.) 1960 *Incompressible Aerodynamics*. Oxford University Press.

VON MISES, R. 1945 *Theory of Flight*. McGraw-Hill.

WU, T. Y. 1962 Flow through a heavily loaded actuator disk. *Schiffstechnik.* **9**, 47, 134.